Universidade de Lisboa

Faculdade de Ciências

Departamento de Biologia Animal

Comparison of brain and cranial nerve morphology between eyed surface fish and blind cave fish of the species *Astyanax mexicanus*

Fábio Ribeiro Rodrigues

Mestrado em Biologia Evolutiva e do Desenvolvimento

2013

Universidade de Lisboa

Faculdade de Ciências

Departamento de Biologia Animal

Comparison of brain and cranial nerve morphology between eyed surface fish and blind cave fish of the species *Astyanax mexicanus*

Fábio Ribeiro Rodrigues

Dissertação orientada por Doutor Yoshiyuki Yamamoto (UCL)

Orientador Interno: Profª. Doutora Sara Magalhães (CBA/FCUL)

Mestrado em Biologia Evolutiva e do Desenvolvimento

2013

Acknowledgements/Agradecimentos

There are several individuals that have to be thanked, and perhaps some of them will not be listed, but I will do my best.

To Dr Yoshiyuki Yamamoto, who accepted me in his lab, supported my stay here and opened a lot of possibilities for my future. No words can express my gratitude.

To Dr Mathilda Mommersteeg (Tilly), for all her help in dealing with some parts of the scientific process, for the sectioning and Amira) and for the moral support (in the form of caffeine or frappuccino).

To Mark Hajawi from Tim Arnett's lab, that helped us with the micro-CT scanning.

To Monica Folgueira, for the help with the confocal imaging, and all the corrections she made!

To Elizabeth Ward (Lizzie) from Claudio Stern's lab, for her availability to teach me how to operate the OPT.

To Dr Brian Metscher, who even from afar tried to help me the best way he could.

To Simone Villari, for all his patience and support which were indispensable to get me through this year.

Ao Prof. Dr. Élio Sucena, por todo o apoio prestado enquanto me encontrava no estrangeiro, bem como pelas recomendações que enviou. Muito obrigado!

À Prof.ª Dr.ª Sara Magalhães, pela ajuda e disponibilidade que demonstrou e por todas as correcções e indicações dadas!

À Prof.ª Dr.ª Sólveig Thorsteinsdóttir, pelo apoio prestada à distância e pela disponibilidade em ajudar no que fosse preciso.

A todos os restantes Professores que construíram e fazem parte deste Mestrado, um grande obrigado pelas oportunidades que dão pois, mesmo com todas as adversidades, principalmente económicas, conseguem abrir portas a um mundo de possibilidades e, mais importante ainda, conseguem transmitir a sua paixão 365 dias por ano.

Finalmente, aos meus pais e irmãs, que me apoiaram em tudo durante este ano e, mesmo que difícil, fizeram o possível e impossível para me ajudar. Um grande obrigado!

Sumário

O Sistema Nervoso Central (SNC) de qualquer vertebrado desenvolve-se a partir de uma estrutura semelhante, fazendo uso dos mesmos factores. A placa neural embrionária, através da acção coordenada de Wnts, FGFs, Sonic Hedgehog e BMPs, é padronizada nos seus eixos Antero-Posterior e Dorso-ventral. Estes mesmos factores desencadeiam o desenvolvimento de organizadores secundários no sistema nervoso que vão actuando de uma forma gradualmente mais localizada. Como resultado, cinco vesículas cerebrais são formadas: Telencéfalo, Diencéfalo, Mesencéfalo, Metencéfalo e Mielencéfalo. Os mesmos factores actuam posteriormente no controlo da proliferação de células progenitoras neurais.

Esta organização corresponde ao arquétipo cerebral de qualquer vertebrado a partir da qual toda a diversidade morfológica que se verifica na natureza é gerada. Pequenas modificações em qualquer um destes três momentos do desenvolvimento do SNC (padronização, regionalização e neurogénese, respectivamente) podem alterar a morfologia final do encéfalo. No caso dos teleósteos e peixes cartilagíneos, regiões específicas do cérebro apresentam expansões relativamente ao resto do cérebro conforme o *input* sensorial – a título de exemplo, os tubarões apresentam geralmente cerebelos mais desenvolvidos dado o grau de mecano- e electrorrecepção, enquanto teleósteos apresentam maiores expansões do tecto óptico, que responde ao input visual. Parece de facto haver uma correlação entre a alteração de diferentes regiões do cérebro e o nicho que as espécies ocupam. Estas observações estão de acordo com a hipótese de Evolução em Mosaico, que afirma que diferentes regiões do cérebro alteram-se conforme as exigências ecológicas do meio que a espécie ocupa. Esta teoria contrapõe-se à ideia de que constrangimentos no desenvolvimento do cérebro levam à modificação coordenada do desta estrutura como um todo. No entanto, para perceber como o SNC evolui, é necessário mais que descrever diferenças anatómicas e correlacioná-las com o meio. É igualmente indispensável entender quais os mecanismos responsáveis por estas alterações, quando é que estes foram modificados e que forças levaram à retenção dessas alterações. Infelizmente, os modelos animais mais utilizados não nos garantem respostas a todas estas perguntas.

A espécie de teleósteo *Astyanas fasciatus mexicanus* é originária da América Central e é composta por populações de superfície com um fenótipo perfeitamente similar ao de outros peixes. Esta espécie apresenta também um morfotipo cavernícola que, embora tenha divergido significativamente do seu ancestral, não atingiu o isolamento reprodutor. É, portanto, possível gerar híbridos férteis ao cruzar ambos os morfotipos. A colonização das cavernas terá ocorrido há cerca de 8 milhões de anos, tendo havido segunda onda de colonização mais recente estimada nos 3 milhões de anos que originou outras populações. No meio cavernícola, as populações não são predadas e encontram-se num ambiente relativamente estável. Contudo, este ambiente pode ser particularmente hostil dada a falta de alimento durante a estação seca e à hipoxia do meio aquático. Todos estes factores poderão ter gerado pressões selectivas grandes o suficiente para permitir divergências genéticas e fenotípicas entre populações de superfície e cavernícolas. Não se pode excluir o papel da deriva genética, pois dada a escassez de alimento e o isolamento, é de prever que as populações estejam sujeitas à acção de *bottlenecks* periódicos, promovendo a erosão da diversidade genética destes grupos. Estas populações cavernícolas evoluíram independentemente um fenótipo convergente: perda de pigmentos, expansão da linha lateral craniana, maior número de papilas gustativas e degeneração dos olhos. Todas estas características, bem como a possibilidade de fazer análises moleculares, tornam esta espécie num excelente modelo para estudar evolução do SNC.

A expansão da linha lateral permitiu aumentar a capacidade de mecanorrecepção deste morfotipo, compensando a perda da visão que é tradicionalmente considerada um sentido dominante em teleósteos. Sabendo que a degeneração dos olhos resultou numa redução do tecto óptico – região do cérebro que responde a estímulos visuais –, é expectável que o incremento no *input* proveniente da linha lateral tenha resultado em modificações de outras regiões do cérebro. Há, no entanto, várias outras modalidades sensoriais (olfacto, paladar, tacto) que poderão ter sido modificadas no ambiente cavernícola, à semelhança da linha lateral, permitindo que indivíduos consigam lidar com as adversidades deste meio.

Qualquer informação sensorial é transmitida ao cérebro através de nervos cranianos. Estes são tipicamente doze, mas em vertebrados basais, como teleósteos, estes são dez (excluem-se os nervos XI, acessório e XII, hipoglossal). No entanto, dada a capacidade de mecanorrecepção deste grupo de vertebrados, estes possuem ainda os nervos anterior e posterior da linha lateral. No caso de *Astyanax*, sabe-se que houve uma redução do nervo óptico (II) – o que está em parte associado à redução do seu respectivo órgão sensorial. Nada se sabe em relação aos outros nervos.

Desta forma, definimos como objectivo deste projecto descrever morfologia dos nervos cranianos e do cérebro em ambos os morfotipos, de forma a perceber como é que o ambiente cavernícola afectou quer o *input* sensorial quer os respectivos centros no cérebro. As medições foram realizadas em indivíduos criados no mesmo ambiente e em dois estadios, a cinco dias depois da fertilização (larvas) e a um ano de idade. A medição robustez dos nervos cranianos e o volume de diferentes regiões do cérebro nestes dois estadios permitiu comparar diferenças definidas durante o desenvolvimento e outras que pudessem aparecer mais tarde na ontogenia.

As medições de volume do encéfalo foram feitas através de microtomografia computacional (micro-CT), uma técnica de imagiologia baseada em raios-X. Esta permitiu realizar reconstruções 3D do encéfalo dos peixes em ambas idades após um tratamento com ácido fosfotúngstico para marcar tecidos não mineralizados. Através destas reconstruções, foram medidos os volumes do cérebro, bolbo olfactivo, telencéfalo, tecto óptico, hipotálamo e cerebelo. Esta técnica permitiu ainda a medição dos nervos cranianos de espécimes adultos. Para medir e comparar nervos cranianos das larvas, fez-se um ensaio imuno-histoquímico para tubulina-α acetilada, marcando os axónios destes nervos para serem visualizados em microscopia confocal. As imagens obtidas foram usadas para fazer reconstruções 3D dos nervos cranianos de modo a medir as respectivas áreas de secção.

Como resultado, reportamos que para além do nervo óptico, os nervos associados com os músculos do olho (oculomotor e troclear) têm também um menor diâmetro no morfotipo cavernícola. Para além disto, os nervos trigémeo e linha lateral anterior têm uma maior área de secção no mesmo morfotipo, representando um possível incremento no *input* somato- e mecanossensorial, respectivamente. O cérebro da forma cavernícola aparenta ter um menor volume que o dos peixes de superfície, o que pode representar uma adaptação importante ao ambiente hipóxico e à falta de recursos alimentares.

Ao contrário do que sugerido por trabalhos anteriores e contra as expectativas de uma coordenação entre modificações sensoriais e cerebrais, o telencéfalo, hipotálamo e cerebelo aparentam ser relativamente menores neste morfotipo. Verificou-se que o tecto óptico, a região do cérebro que responde ao *input* visual, se encontra subdesenvolvido. Isto é verificado ainda na fase larvar, evidenciado que esta redução pode ser uma característica já fixa no código genético da população cavernícola. O bolbo olfactivo aparenta representar uma maior fracção

do cérebro no morfotipo cavernícola. Muito embora a análise efectuada não revele diferenças no hipotálamo, telencéfalo e cerebelo deste morfotipo, é importante referir que trabalhos anteriores descrevem alterações no número de neurónios que constituem os núcleos cerebrais nos peixes cavernícolas, causando modificações comportamentais. Assim, nesta fase incipiente do processo de especiação, as principais diferenças no SNC de ambos os morfotipos podem assentar nos diferentes núcleos cerebrais, sendo estas talvez mais relevantes para garantir a sobrevivência da forma cavernícola num ambiente hostil.

Palavras-chave

Astyanax mexicanus; Evolução; Cérebro; Nervos Cranianos; micro-CT

Abstract

Understanding how the brain evolves in response to new environmental situations is key to comprehend not just the developmental mechanisms underlying the generation of variability in brain patterns, but also to understand how the animal's perception and mental representation of their environment evolves. With this idea in mind, we described the differences in cranial nerve and brain morphology between the eyed surface form and the blind cave of *Astyanax fasciatus mexicanus* using micro-CT technology. This is, to our knowledge, the first time this method is employed for neuroanatomical studies. Comparisons were performed at both five day old and one year old fish. Our results show a topological conservation of cranial nerves in both morphotypes with significant reductions in visual related nerves in the cavefish along with a reduction in the optic tectum. We also found an increased robustness of the trigeminal and anterior lateral line nerves, responsible for somato- and mechanosensory input, respectively. At 5 dpf the surface fish brain is bigger than the cavefish and no differences were found between different regions. The overall adult brain volume of cavefish is approximately 20% smaller in the cavefish, which is also accompanied by a reduction of its telencephalic, hypothalamic and cerebellar regions. The olfactory bulb appears to circumvent this trend, showing signs of enhancement. This overall reduction shows that energetic constraints may be of significance in shaping the overall morphology of the brain the cave environment.

Keywords

Astyanax mexicanus; Evolution; Brain; Cranial Nerves; micro-CT

Table of Contents

INTRODUCTION **1**

MATERIALS AND METHODS **6**

Animal rearing and manipulation 6
Micro-CT sample preparation and imaging 6
Volume measurements 7
Lens manipulation 7
Enzyme metallography, paraffin sections and OPT 8
Confocal imaging of Acetylated a-tubulin staining 8
Cranial nerve 3D reconstructions and measurements 8
DiI injections 9
Statistical analysis 9

RESULTS **10**

Lens manipulation in surface fish 10
Enzyme metallography 10
Immunostaining in paraffin sections 11
OPT 12
Confocal imaging, reconstruction and cranial nerve measurements 12
Adult cranial nerve reconstruction and measurements 14
Brain morphology 19

DISCUSSION **27**

Methodology 27
Vision related nerves 27
Olfactory and Octavolateral nerves 28
Trigeminal and Lateral Line modifications 28
Changes in brain shape and morphology 29
The Tectum and Olfactory Bulb 29
The case of the Telencephalon, Hypothalamus and Cerebellum 30
On the origin of CNS differences 31
CNS evolution in Astyanax 32

REFERENCES **33**

SUPPLEMENTS **38**

Material and Methods 38
Acetylated α-tubulin staining for Micro-CT imaging *38*
Acetylated α-tubulin DAB staining *38*
OPT preparation and imaging *39*
Paraffin sectioning, immunohistochemistry and reconstruction *39*
Lens deletion in surface fish *40*
Supplemental Figures 40
Cranial nerve 5 dpf *40*
Ratios of different regions across stages *42*
Ratios at 5 days without the Tectum *42*
Adult Ratios with identical TeO in both Morphotypes *42*

“As long as our brain is a mystery, the universe, the reflection of the structure of the brain, will also be a mystery.”

Santiago Ramón y Cajal

Introduction

For almost a century, scientists have been attempting to describe and grasp the complexity of the system that detects environmental signals and constructs complex behaviours in response to such stimuli. Ever since Santiago Ramón y Cajal, we have come to understand how different types of neurons are distributed in several nervous tissues and what is the functional significance of such organisation. The central nervous system (CNS) develops, like all other systems, through complex signalling networks that are responsible for (i) its patterning, (ii) for its further compartmentalization and, finally, (iii) for the neurogenic process [1-5]. Although these networks are well conserved across all vertebrates, they may have different outcomes based on some variances, such timing or duration of activity [2, 6-9].

As a consequence of such alterations, a large array of adult brain morphologies arises in all vertebrate lineages which, astoundingly, derive from the same embryonic *bauplan*. These different adult morphologies appear to correlate with both sensory and ecological demand of each species niche. Cartilaginous fishes for instance, seem to have enhanced olfactory bulbs (OBs) and cerebellum. The former is an anterior region responsible for olfaction and the latter performs sensory-motor integration and processes mechanoreceptive input [10]. In most teleosts however, the optic tectum (TeO), which receives direct input from the eyes, is, in most teleosts, a dominant sensory brain region [10, 11]. Modifications like this are detectable in smaller phylogenetic scales and can also be correlated with the animal’s environment. Some species of carps (Cyprinids) rely mainly on gustatory input to cope with their environment, thus having specifically enlarged brain nuclei in the hindbrain to respond to such stimuli [10].

Specific sensory needs appear to have a strong influence on the degree of morphological change that the brain undergoes. This is in agreement with the theory of Mosaic Brain Evolution, which suggests that overall brain morphology can be changed by the expansion/reduction of specific brain regions independently of others. Another theory considers how functional association of these different parts constrains the levels of plasticity in brain morphology, hence its name Developmental Constraints theory. It proposes that such constraints cause coordinated changes between regions, resulting in larger or smaller brains which are scale-up/down versions, respectively, of the ancestral morphology. Both theories can be largely explained by specific genetic changes that affect CNS development [5, 10, 12]. Such alterations cannot proceed on their own, as modifications in specific brain regions should be in agreement with changes in both sensory input and effector output. The structures responsible for conveying afferent information to the brain as well as the appropriate efferent output are termed Cranial Nerves (CNs).

CNs have both a motor and sensory component and their nuclei develop in the hindbrain and midbrain. These nuclei exist in different rhombomeres and produce pioneering efferent axons which will exit the brain and follow paths towards specific muscles/structures. Afferent axons from peripheral organs find their way into the brain and develop sensory ganglia outside of the brain. To certain extent and not always, both motor and sensory components bundle together. Functionally, CNs communicate external signals to the brain but also transmit motor responses and control several different “autonomous actions” such as breathing and swallowing [13]. There twelve CNs: Olfactory Nerve (I); Optic Nerve (II); Oculomotor, Throchlear and Abducens (III, IV and VI, respectively), all controlling different eye muscles; Trigeminal (V), jaw muscle innervation and associated structures (like teeth); Facial (VII), responsible for gustatory

information and facial muscle control; Acoustic or Octavolateralis (Ole) in fish (VIII); Glossopharyngeal (IX), pharynx innervation; Vagus (X), visceral innervation; Accessory (XI), neck muscles; and Hypoglossal (XII), tongue muscle innervation. This general CN organisation is shared by most vertebrates, but there are variations beyond this description. Fish for instance do not have CN XI or CN XII, but they possess a nerve that transmits input captured by mechanoreceptive structures termed neuromasts. The neuromasts are organised into the Lateral Line System (LLS) and its sensory information is directed to the brain through the Anterior and Posterior Lateral Line Nerves (ALLN and PLLN, respectively) [10, 14]. The sensory/afferent portion of some CNs develop through contributions of neural crest and neurogenic placodes, forming sensory ganglia and specific types of neurons (sensory bipolar neurons) [10]. It is also expected that these structures, as well as their respective processing centres, can undergo modifications as a result of ecological demands.

Intrinsic CNS differences between organisms result from the "tinkering around" with these different "modules" (both at the brain and at the CN level), which are further refined by years of natural selection. But studying the evolution of this system requires the appropriate set of questions ("What?", "When?", "How?", and "Why?") [8] and a model organism that can provide answers. *Astyanax fasciatus mexicanus*, a fresh water fish species, has particularities that make it an exceptionally good model to answer such questions. This species consists of an eyed surface fish, widely distributed in northeastern Mexico and southern USA, and several eyeless cave populations (cavefish) throughout Central America [15]. This species belongs to the order Characiformes (family Characidae) and the first *Astyanax* cavefish were discovered in limestone caverns in northeastern Mexico [16]. They have been described as different species, but due to their interfertility, surface and cave forms are now considered morphotypes of the same species [17].

Distinct cave populations display the same phenotype that has evolved independently in each cave. This is supported by the isolation of each cave and by the intricate topography of the region that would not allow contact between caves. Genetic analysis also support the multiple origin hypothesis, particularly complementation crosses between different cavefish which rescue the surface phenotype, and intra-/inter-population variation studies [15, 18, 19]. Several mitochondrial and nuclear DNA analyses exposed the complex and controversial history of this species: periodic bottlenecks in cave populations; high allelic variation in the epigean populations compared to the low allelic diversity in cave populations due to the low founding number of individuals [18]. The most recent consensus is that the Mesoamerican cave populations were originated by two waves of ancestral epigean forms coming from South America. The first wave, which occurred between 3.1 Million years ago (Mya) and 8 Mya, gave rise to the cave populations of the Sierra de El Abra, a limestone mountainous complex that allowed stream capture and isolation of several surface fish. The second wave, 2.1 Mya, founded the Micos and Guatemalan populations which are 90 km away from the El Abra region (genetic studies confirm their dissimilarity and age difference)[18]. Introgressive hybridization events between cave populations and surface ones can occur frequently in some caves or rarely in others. This depends on the caves' altitude. The higher the caves, the more isolated they are, making hybridization an uneven (if not impossible) phenomenon throughout time [18].

The Pachón cavefish are a particular population originated in the first wave of invasion and have experienced very few crosses with surface fish [18, 20, 21]. They show one of the highest levels of genetic differentiation from surface fish, which is a likely result of its isolation and low funding number of individuals [22]. Genetic drift may have shaped some of its traits, reducing its variability and increasing its genetic differentiation from river populations, all in cooperation with selective forces [18, 20-23].

Cavefish, as well as their surface counterparts, can adjust to life in the laboratory without much hassle. They can be raised on a simple diet and spawning can be induced every other week by raising the water temperature. Embryos are easily collected and raised, and all important events of their development can be followed due to their transparency. They hatch roughly at 24 hours post-fertilization (hpf) and start actively eating brine shrimp at 5 days post-fertilization (dpf). Usually in 4-6 months, the individuals become fully mature and ready to mate [19]. Their proximity with zebrafish (*Danio rerio*) allows the use of some genetic and molecular tools developed for the latter, from morpholinos to transgenesis [15]. The ability to generate fertile hybrids between morphotypes also allows to study the genetic basis of their phenotypic differences.

For these reasons and given the detailed information about *Astyanax* origins and phylogeny, this species appears to be an excellent model to study CNS evolution. Unorthodox models like *Astyanax* not only allow us to overcome some of the limitations of other vertebrate models, but also open a wide range of new questions that have not been exhaustively depicted in other organisms, providing more interesting challenges to modern day science.

Previous works have documented differences between surface and cavefish neuroanatomy. The loss of visual input was compensated by the enhancement of other sensory systems of the cavefish, namely the LLS and Taste Buds (TBs) (chemoreception) [15, 19, 24-26]. The neuromasts are present in a higher number in the cavefish [27]. They are also larger (with a respectively larger sensory area) and have a longer cupula, which allows cavefish to be more sensitive to hydrodynamic stimuli [28, 29]. The LLS may be of crucial importance in the cave environment, allowing habitat exploration and orientation through a hydrodynamic representation of the environment [29-31]. In regards to chemoreception, TBs are not structurally different between surface fish and cavefish. Yet, some specific TBs in the cave morph contain significantly more axons than those of the epigean morph, which suggests an improvement of this sense [32]. This is caused by the expansion of the expression domain of *sonic hedgehog* (*shh*) at the anterior embryonic midline, which is also responsible for lens apoptosis in the cavefish [26, 33]. The auditory system does not differ between both morphs [34]. In regards to olfaction, which was also expected to be enhanced, it has been shown that olfactory projections to the telencephalon do not differ from other teleosts [35].

Previous authors have described the cavefish brain as more “slender and elongated” than the surface fish’s brain [36]. The pallial and subpallial (dorsal and ventral telencephalic subdivisions, respectively) organisation of both morphs does not diverge substantially [36]. Previous reports have hypothesized an enlarged telencephalon in cavefish [37], an idea which was further reinforced by demonstrating the influence of Shh in the developing forebrain. Shh not only increases cell proliferation in the hypothalamus, but also drives the specific increase of subpallial inhibitory GABA-ergic interneurons that migrate to the OB – located anteriorly to the telencephalon [38, 39]. This suggests that the cavefish olfactory bulb may have suffered some modifications. It also points to probable modifications in the gustatory input, considering that the hypothalamus is a relay centre for this information [39]. The hypothalamus is also the main neurosecretory centre in the vertebrate brain, responsible for hormonal regulation necessary in several homeostatic and behavioural responses. It has also been shown that this structure plays a pivotal role in aggressive behaviour and feeding behaviour [10, 40].

The TeO is a highly stratified portion of the brain of vertebrates which responds to visual and somatosensory input [10, 41]. The correspondent structure in mammals is the superior colliculus [10]. The cavefish TeO appears to be underdeveloped, a hypoplasia most likely caused by the lack of visual input [42, 43] which is already evident at 5 dpf [44]. The first actual test to this hypothesis was performed by Schmatolla [42] through a comparative study between the *Astyanax* river fish, its hypogean form and zebrafish, in both larval and adult stages. He reported

an already hypoplastic TeO at 7 dpf (a reduction of about 55%) in the cave form compared to the surface embryo of the same age. In the adult (over 1 year old), this reduction was still visible (and still of about 50%). Schmatolla also describes a higher density of rounded neurons in the periventricular layers of the adult cavefish TeO, whereas the same layer in the surface fish has neurons with a pyriform shape and have processes that extend into the TeO, suggesting lack of differentiation of neural cells in the cavefish tectum. After performing optic cup extirpation in the river fish before the optic nerve developed (18 hpf), there was a 27.9% reduction in the contralateral TeO when compared to the normal ipsilateral side. After raising the river fish in the absence of light (an experiment which yield no differences in TeO mass), Schmatolla concludes that the innervation itself is required to boost TeO's development, but the "natural denervated" state of the hypogean morph is somewhat more hypoplastic than the "artificially denervated" TeO of the surface fish. Other experiments have corroborated these findings and explained the role of the lens/eye degeneration in TeO hypoplasia. Through lens transplantation from a surface embryo to its cave counterpart [33, 45, 46] Soares et al. [47] showed a 13% increase in volume and 8% increase in neuron number in the contralateral TeO of the operated eye in comparison to the ipsilateral. The surface lens partially rescued the ganglion cell layer of the retina, whose neurons extend their axons to the TeO, forming the optic nerve [47]. However, this rescue does not allow complete tectal restoration in the adult cavefish and optic cup extirpation in the epigean embryo does not phenocopy the cavefish TeO [42, 47].

Not many other brain regions have been thoroughly investigated in this particular species. The hindbrain and its CN nuclei could provide very interesting information about CNS evolution "in the dark". As it has been reported, some fish species that rely on gustatory input to explore their surroundings (like carps, goldfishes and catfishes) have more TBs not only in the head region but also inside the mouth. As a result, CNs that relay this information to the brain (Facial, Glossopharyngeal and Vagus) are more robust and their respective nuclei are also increased in volume [10]. Considering the changes in cavefish's sensory organs, there is reason to think that modifications in their CNs and respective brain centres may represent important adaptations to their habitat. In fact, recent experiments have shown the importance of the enhanced LLS in the cave environment, which elicits an attraction behaviour to high vibrations that helps cavefish finding food, a scarce resource in caves [48-50].

In summary, lack of visual information causes hypoplasia in the cavefish's TeO and there may be hypertrophied nuclei/brain regions in the cavefish brain that respond to enhanced sensory input. So, in *Astyanax*, can these differences be solely due to neural plasticity [51], or has (micro)evolution fixed these traits in the cave morphotype? Previous works state that early brain specification does not differ between surface and cavefish (with the exception of *Pax6* expression domain in the optic primordia region which is larger in the surface fish embryo) [47]. Thus, neural plasticity and the "sensory environment" of the cavefish may account for the differences in brain volume and shape that we find in this morphotype. With this question in mind, we aimed to understand how the cave environment affected both the sensory input and the brain's overall morphology and organisation by comparing the cavefish's cranial nerves and brain morphology with those of its epigean counterpart.

For this purpose, different brain regions and CN robustness were measured to look for coordinated modifications between sensory input and its brain centres. We used the 5 dpf as a basal state to compare with our adult fish (1 year post-fertilization, ypf), all reared in the same environment. Five day old larvae start actively finding food and escaping predators. Therefore, some of differences between surface and cavefish larvae up to this stage can be considered as fixed traits, as sensory experience starts after 5 dpf. Comparing both stages could allow us to distinguish between some developmentally fixed traits and neural plasticity.

Serial sections of an organism can be used to measure volumes of particular organs. This a laborious process which involves modification of the samples, which in turn could conceal subtle volumetric differences. Therefore, the best method to estimate volumes would involve a non-invasive whole-mount procedure. Optical projection tomography (OPT) is one of such methods. It is based on visible light transmission through a transparent sample which has been stained specifically for a structure [52]. Even if this method had worked well for the CNs of 5 dpf larvae, it could not be applied to adult fish due to the transparency requirement. For this reason, x-ray based micro-computed tomography (micro-CT) was chosen. Not only it allows an easy staining method for soft tissues (including both brain and CNs) but it works fairly well in both adults and larvae [53, 54]. As for CN detection and measurement, by using an enzyme metallography procedure it would be possible to trace and measure these structures in the larva [55]. The results obtained would allow the careful selection and measurement of brain volumes and CNs without causing any damages to the samples. Unfortunately, due to setbacks with the technique, CN measurements in 5 dpf stage were made in 3D reconstructions of images obtained through confocal microscopy. This is, to our knowledge, the first time this technique is employed to perform neuroanatomical descriptions an organism

With this method, differences were found in the adult and 5 dpf fish's whole brain volume, but also in the olfactory bulb and TeO of both adult morphotypes. The data gathered does not support previous suggestions of increased telencephalic and hypothalamic volumes and no differences in cerebellar volume were found either. The CN measurements revealed changes in input pathways, particularly trigeminal and LLS, and also demonstrate reductions of vision related nerves. We thus supply evidence of changes in sensory input and brain volume reduction in *Astyanax* cavefish, the latter being a likely result of energetic constraints.

Materials and Methods

Animal rearing and manipulation

The *Astyanax* lab populations came from William Jeffery's laboratory at the University of Maryland, College Park, MD, USA. The surface populations are raised descendants of individuals collected in Balmorhea Springs State Park, Texas, whereas the cavefish populations are descendants of individuals caught in Cueva de El Pachón in Tamaulipas, Mexico. No other cavefish populations were used in this study. All adult individuals were maintained in the same conditions: 19-21°C in a 14:12 hours light:dark cycle; spawning was induced by raising the temperature to 24.5-25.5°C and embryos collected, washed in E2 medium and incubated at 24.5°C. When they reached the desired stage: they were anesthetized in ice; washed once in PBS 1x and then fixed in 4% paraformaldehyde (PFA) overnight at 4°C; progressively dehydrated to methanol and stored at -20°C.

After 5 dpf, larvae were fed with brine shrimp twice a day and after 14 dpf they were transferred to larger container for faster growth. At 30 dpf, the juvenile were transferred into the tanks and fed with commercial food. The adult individuals used in this study, both Pachón and Surface, were exactly the same age (1 year old). All individuals were anesthetized in a tricaine solution, weighed and measured (from the tip of the mouth to the tip of the tail), and then sacrificed through a cut at the base of the skull. The heads were separated from the rest of the body (the cut being made behind the gills) and then fixed in PFA for 24 hours at 4°C before dehydration to methanol and storage at -20°C.

Micro-CT sample preparation and imaging

Samples previously fixed were prepared for Phosphotungstic Acid (PTA) (Sigma) staining as described by Metscher [53]. PTA gives contrast to non-mineralized tissues, including the CNS, allowing to detect and reconstruct the latter after imaging. A 1% PTA Stock Solution in water was prepared, a portion of which was used to make a 0.3% PTA solution in 100% Ethanol (Sigma). Samples, both adults and 5 dpf larvae, were then serially dehydrated to 70% Ethanol and transferred into the 0.3% PTA solution in Ethanol. Penetration time varied with age and size of the samples. Larvae took 2 days to stain and for both surface and Pachón cavefish heads, it was necessary to remove a small part of the dorsal cranial bone to facilitate the penetration of the staining agent, resulting in a staining time of 2 weeks. For the adults, the PTA solution was changed every 4 days. Samples were mounted in a 70% ethanol medium in polypropylene micropipette tips (Gilson), sealed and capped with Blu Tack (Bostik)[53].

The imaging was performed with Skyscan 1172 high-resolution Micro-CT scanner (Bruker-microCT, Kontich, Belgium), using a tungsten source (Hamamatsu 100/250). Adult heads were scanned at 59 kV and 149 mA (8W) with Al 0.5 mm filter, whereas 5 dpf fish were scanned at 40kV and 100uA (4W) without filter. Source-sample distance was set at 36 mm for 5 dpf fish and 94.53 mm for the adult. Projection images were taken every 0.3 of rotation and then saved as 16-bit files. Using Bruker microCT's reconstruction software NRecon, these projection images were converted into virtual z-sections in Bitmap format. All the adult image files had a 9.95 µm pixel size whereas the images for the younger fish had 1.18 µm pixel size. Total scanning time for each adult head was approximately 50 min with a 10 min reconstruction time. Total larval scanning times were approximately 1 hr and 20 min with a 30 min reconstruction time.

Volume measurements

Figure 1 – Reconstructed micro-CT scan image of a virtual section of a 5 dpf Pachón larva through the midbrain. The red region represents a ROI selection identical to what was performed in all scanned samples. The ROI selected in this picture corresponds to the TeO.

The reconstructed Bitmap image files from each individual were then loaded into Bruker-microCT analyzing software CTAn 1.12.0. For each set of images, the whole brain and specific brain regions were selected as Regions of Interest (ROI) across the whole dataset (Fig.1). This selection yielded entire Volumes of Interest (VOI) that were binarised to threshold the grey values that corresponded to the structure of interest. For all brain structures and across all individuals of the same age, this threshold was kept the same to allow comparable results. After binarisation, the software could perform a 3D analysis of the whole VOI previously binarised.

This method was used to measure the whole brain volume as well as some of its specific regions. The adult brain was selected from the OB to the beginning of the spinal cord (immediately after the hindbrain, the diameter of the medulla reduced significantly and the bulbous aspect gave rise to a more circular tube). The 5 day larval brain was selected from its most rostral point, right after the nostrils, up to the point where the musculature appeared (spinal cord).

The adult brain regions analysed include the OB, telencephalon, TeO, hypothalamus and cerebellum. At 5dpf, the same regions were selected, with the exception of the OB and cerebellum, which are not evident at this stage. The larval telencephalon was selected from the nostrils up to the diencephalon. In the adult, the OB was defined from the brain's most rostral point to the telencephalon, and the latter was then selected from that point to the beginning of the diencephalon as well. The TeO, right above the ventricle (Fig.1), starts rostrally just on top of the diencephalon and terminates caudally as two lateral structures separated by the cerebellum/hindbrain in adults/larvae, respectively. The cerebellum was selected from the valvula cerebelli (its most anterior part located inside the tectal ventricle) all the way to hindbrain. The hypothalamus was selected from its most caudal point, where its lobes are clearly separated from the rest of the midbrain, to its rostral extremity, just behind the optic chiasma [10].

Lens manipulation

To detect changes associated with sensory experience, we set out to perform lens deletions in surface fish (detailed method in supplements)[46]. Time constraints however, did not allow us to scan matured individuals.

Enzyme metallography, paraffin sections and OPT

Enzyme metallography staining was used to detect CN in the 5 dpf fish [55]. However the method did not work out properly. To solve this issue we also tried to perform paraffin sections and OPT imaging. However problems arose in these methods as well. The detailed procedures used for these techniques are in the supplemental information.

Confocal imaging of Acetylated α-tubulin staining

Due to the high-resolution of the technique, confocal microscopy was used to image CN of 5 dpf fish. For this purpose we performed an immunostaining for Acetilated α-tubulin (Aαt) by using previously fixed fish. These fish were rehydrated to PBT, digested in proteinase K at 40 µg/ml for 30 min at room temperature, post-fixed in PFA 4% for 20 min, and washed in PBT before the 1 hour blocking step (blocking solution: 10% normal goat serum, 1% DMSO, 0.5% Triton-X100 in PBS). Samples were incubated overnight at 4°C in primary antibody (mouse anti-Aαt, Invitrogen) diluted at 1:200 in the same blocking solution. After 4 washes in PBT (30 min each), embryos were incubated (overnight at 4°C) in the secondary antibody (Alexa Fluor 488 goat anti-mouse IgG, Invitrogen) diluted at 1:200. After the final washes, in PBS, the embryos were mounted for confocal imaging: plastic rings were fixed to a glass slide with a silicone glue, where 1% agarose in PBS was added to immobilize the fish that had been properly positioned before cooling. Samples were imaged by scanning laser confocal microscopy (Leica™ TCS SPE), for one channel and with a 4 µm z-step.

Cranial nerve 3D reconstructions and measurements

For adult fish, the cranial nerves were reconstructed from PTA stained heads. The reconstructed tomographic images were halved by selecting every other image, and this new data set was read in Amira 5.3.3 (Visage Imaging) adjusting the voxel z distance for double the original (from 9.95 µm to 19.9 µm). This was done to reduce the amount of computational and graphical power the software would require. Selection and identification of nerves was performed by going through virtual sections in all axes and by using previously published information on CN anatomy in other fish [56-58]. Due to the fact that some of the cranial nerves bundle together and/or that their "entry point" into the brain was hard to detect, not all the cranial nerves were accurately and consistently reconstructed in all the individuals. For this reason, the Abducens (CNVI), Facial (CNVII), Glossopharyngeal (CNIX) and Vagus (CNX) will not be included in this analysis of adult fish. The CNI was easily reconstructed due to its linear path from the nose to the OB. The same can be said for the Optic Nerve, whose path was linearly followed from the eye to optic chiasma. The Oculomotor and Throchlear nerves were followed by tracing them from specific muscles: the former was traced from the Inferior Rectus muscle (located in the ventral posterior quandrant of the eye), even though this nerve is also responsible innervation of the Superior Rectus and Inferior Oblique muscles; the latter was traced from the Superior Oblique muscle, the most rostral-dorsal muscle of the eye. The remaining nerves (Trigeminal, Anterior and Posterior Lateral Line nerves and Octavolateralis) were selected and identified for their relative position, innervation targets and/or entry points. Measurements to all these nerves were made by applying a cutting plane in a specific point of their anatomy: CNI, V, VIII, ALL and PLL were sectioned just after their entry points into the brain; CNII, III and IV were sectioned halfway in their path. After this step, section areas were measured and their values recorded for posterior analysis. Both left and right CNs per individual were measured and their value was then

averaged, yielding a single value per CN per individual. At 5 dpf, fewer CNs were reconstructed in Amira (solely CNII, CNV, CNVIII, ALL, PLL and CNX).

DiI injections

To trace the PLL and ALL nerves, injections of DiI were made at 5 dpf surface and cavefish [47, 59]. All injections were made in PFA fixed fish previously washed in PBS. To allow for more precision, fish were then immobilized in 1% agar in PBS 1x. DiI (Sigma) was dissolved in Dimethylformamide (Sigma) yielding a stock solution of 2mg/ml. The tracer was loaded into glass micromicropipettes and, with a micromanipulator (Narishige) and pressure-injector system (Picospritzer III), the dye was injected into the specific organ. For lateral line tracing, the dye was injected in a particular ganglion: anterior lateral line ganglion (ALLG), located between the eye and otic vesicle, or posterior lateral line ganglion (PLLG), located immediately after the posterior pole of the otic vesicle. After the injections, fish were removed from the agar and left overnight at room temperature in PBS. Afterwards, the staining was checked and pictures were taken in 0.2% agarose in PBS.

Statistical analysis

Whole brain volume measures were either $\log_{10}$ transformed or square rooted if values were below 1 mm^3. This made our dataset comparable through parametric statistical analysis. To test for differences in relative brain size among the two populations the transformed brain volumes were normalized by dividing them by the $\log_{10}$-transformed whole fish volume. The latter was estimated by approximating the fish's volume to that of a prism, using body length, width and height of each individual as sides of a hypothetical rectangular prism. All ANOVA analysis and respective post-hoc (Scheffé) tests were performed in the normalized dataset. This methodology was applied to both 5 dpf and adult fish. For different brain structures to be compared, a normalization step was also required. In this case, as it has been done in previous works [60], we divided the measured volume of each structure by the absolute whole brain volume, thus yielding a ratio. It was with these ratios that the comparative tests were performed. All ANOVA assumptions were verified prior to execution of these comparisons and, in cases where these were violated, non-parametric tests were performed.

For CN robustness measurements, the data was also transformed (square-root), and these results were then normalized by dividing them by the $\log_{10}$-transformed hypothetical surface area of each fish. This surface area was estimated by, again, assuming the fish as a rectangular prism and summing the areas of each face of this volume given by body length, width and height. After ascertaining that there were no differences between left right with a t-test between variables, averaged values were then compared through both parametric (ANOVA) and non-parametric (Mann-Whitney U) tests. At 5 dpf stage, the section areas were not normalized due to lack of the respective body length of individuals. Regardless, their areas were still analysed. All statistical analysis and graphs were done with STATISTICA 11 (StatSoft, Inc.).

Results

Lens manipulation in surface fish

After the experimental procedures, larvae were screened for malformations and/or presence of the lens. Only the desired fish were reared to adulthood or sacrificed at 5 dpf. Unfortunately, due to time constraints, these fish were not analysed for CNS volumetric modifications – they had not reached a desired and comparable body length with that of the adult fish used for the other measurements.

Enzyme metallography

In order to compare CN differences between surface and cavefish, we first tried to produce accurate 3D reconstructions through micro-CT imaging. For that we performed an enzyme metallography immunostaining for Aαt. This staining forces the precipitations of silver in the area neighbouring the location of the secondary Horseradish Peroxidase (HRP) conjugated antibody, thus allowing x-ray contrast. These silver deposits can be observed with visible light under the dissecting microscope (Fig.2), but the micro-CT was unable to detect any silver deposits. This method was performed several times with adjustments (Supplements), none of which were successful. Also, the staining never penetrated enough to see the entry point of the CNs into the hindbrain – only the most superficial braches were easily stained.

Figure 2 – 5 dpf Steinhardt (Chica) cavefish stained for Aαt using the EnzMet™ kit to create x-ray detectable silver deposits in CNs which would allow 3D reconstruction through micro-CT imaging. Scattered silver deposits can be found throughout the surface of the larva and, in darker tones, some of the CNs are visible, particularly CNV and ALLN branches around the eye (scale bar, 200 µm).

To see if the antibody penetration problem was due to the secondary antibody's molecular weight, we performed DAB staining following the same protocol and an alternative one. As the images show (Fig.2), more CNs can be seen, but not by their entry point into the hindbrain. After several other attempts to make this method work, we decided to try sectioning the larvae, staining the sections for the same antibody and manually reconstruct the sections.

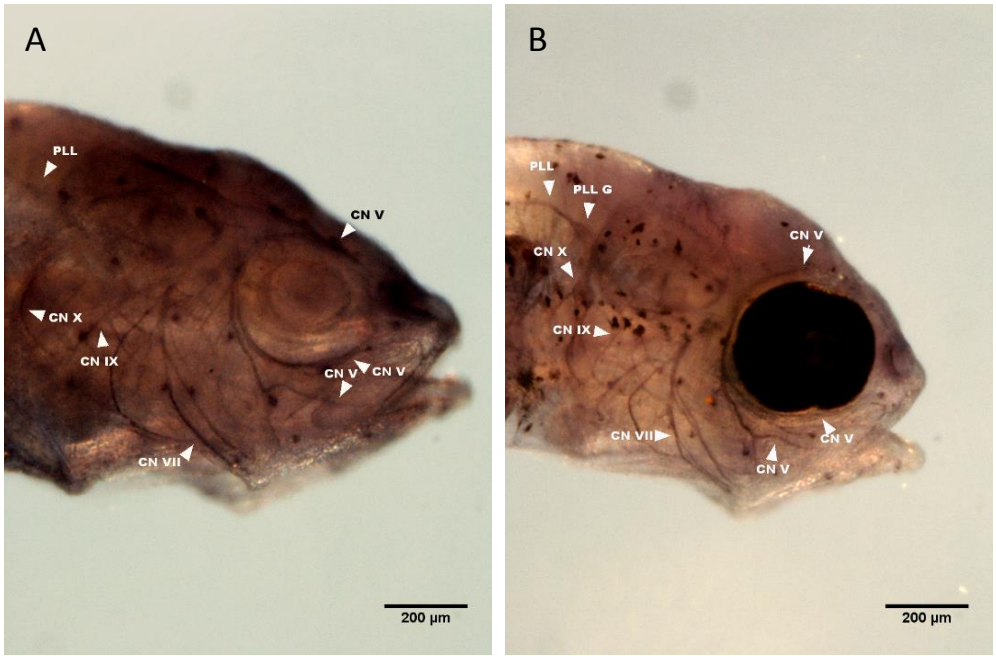

Figure 3 – DAB staining for Aαt in 5 dpf Pachón cavefish (A) and surface fish (B). This staining allowed to identify more CNs than with the EnzMet™ (indicated in the images). However the penetration still remained an issue (scale bar, 200 µm).

Immunostaining in paraffin sections

After determining the right primary antibody dilution (1:50 Aαt in TNB), all 5 dpf larval sections were imaged. However some of the sections were detaching from the glass slides (see Fig.4). After controlling for possible mistakes and errors that could have been made throughout the entire protocol (see supplemental information), the problem still arose. Even though not all sections had this problem, the ones that did would render inaccurate and misaligned reconstructions, upon which no measurements could reliably be performed.

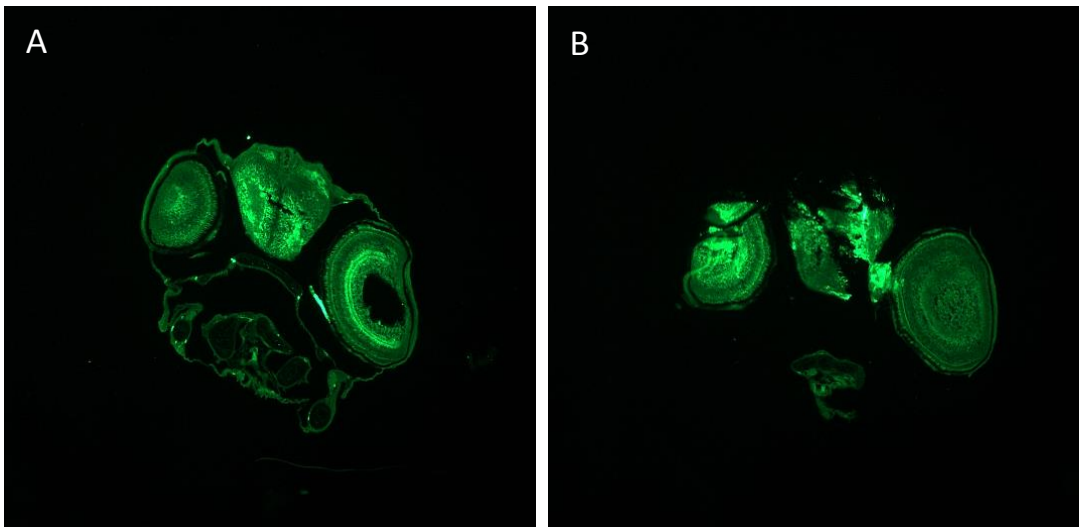

Figure 4 – Example of Aαt staining with secondary Alexa Fluor® 488 in a 5 dpf surface fish. The first image (A) shows the normal aspect of a section, with part of the optic nerve tract in the eye at the right side. The second image (B) demonstrates how the tissue looks like when it detaches from the slide.

OPT

To test this procedure, we injected Fluorescent Dextran Amine (FDA) and Rhodamine Dextran Amine (RDA) into 5 dpf surface and Pachón larvae brain and then proceeded with the sample treatment and imaging. The results obtained showed a staining much weaker than anticipated (Fig.5). Even though the images obtained could serve some purposes, the long laborious sample preparation yielded images which could not serve for the 3D reconstructions of the brain. On top of that, problems with the OPT scanner filters would not allow us to image CNs properly either.

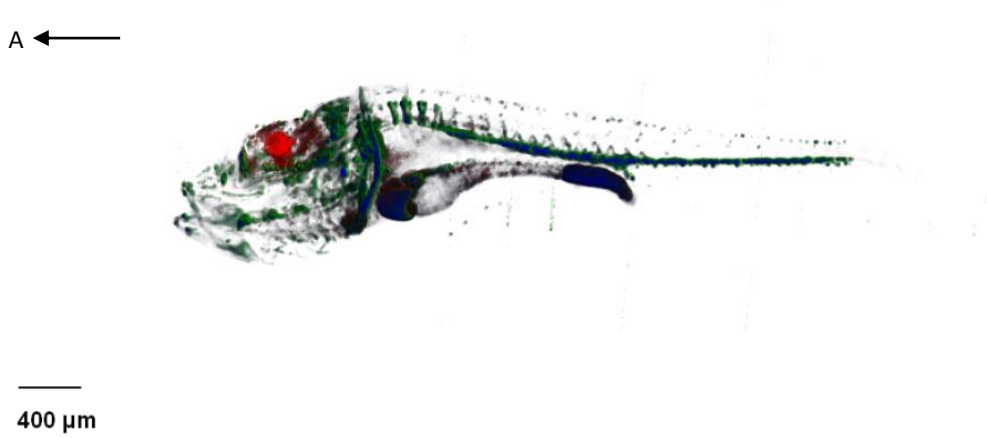

Figure 5 – OPT reconstruction resulting from the FDA and RDA injections in a 5 dpf Pachón cavefish. The arrow in the top left corner indicates the anterior direction. FDA (green) was injected into the hindbrain and from there it spread to other regions of the body. RDA (red) was injected into the tectal ventricle, and it did not spread out beyond the midbrain. The blue regions were imaged with the anatomy channel, which detects tissue auto-fluorescence and reconstruct an overall outline of the sample.

Confocal imaging, reconstruction and cranial nerve measurements

After immunostaining for Aαt and confocal imaging, we were able to reconstruct the cranial nerves from surface (n=4) and cavefish (n=5) at 5 dpf stage. Regrettably, the staining was not visible with a fluorescent dissecting microscope. With the confocal microscope, the signal was detected, but the gain had to be increased significantly, which in turn increased the background noise (Fig.6 A and B). Reconstructions of the most evident CNs were still performed using Amira 5.3.3 (Fig.6 C and D). These include CNV, ALLN, CNVIII, CNIX, PLLN and CNX, all of which, with the exception of CNIX, were measured at a level close to their entry point to the brain. Due to the weak signal, some of the CNs appear more dotted, particularly the CNX and the PLLN (Fig.6). When virtual section planes were applied to these nerves, the generated surfaces were patchy. Nevertheless, and as this was the case for all the samples, measurements were made and compared.

From a topological point of view, the nerve's paths do not seem to differ between both morphotypes. There are some differences in the CNV and ALLN around the eye orbit (their tracts are more apart in the cavefish). The distinction between the CNV and ALLN branches was made after DiI injections to the ALL ganglion – the ALLN branches are connected to the neuromasts (Fig.7). Section area comparisons of the different nerves at this stage did not yield significant differences between both morphs (Mann-Whitney U, $p>0.05$). The graphs, though, suggest that such differences might exist, particularly in the CNX (see S.Fig.1 and 2).

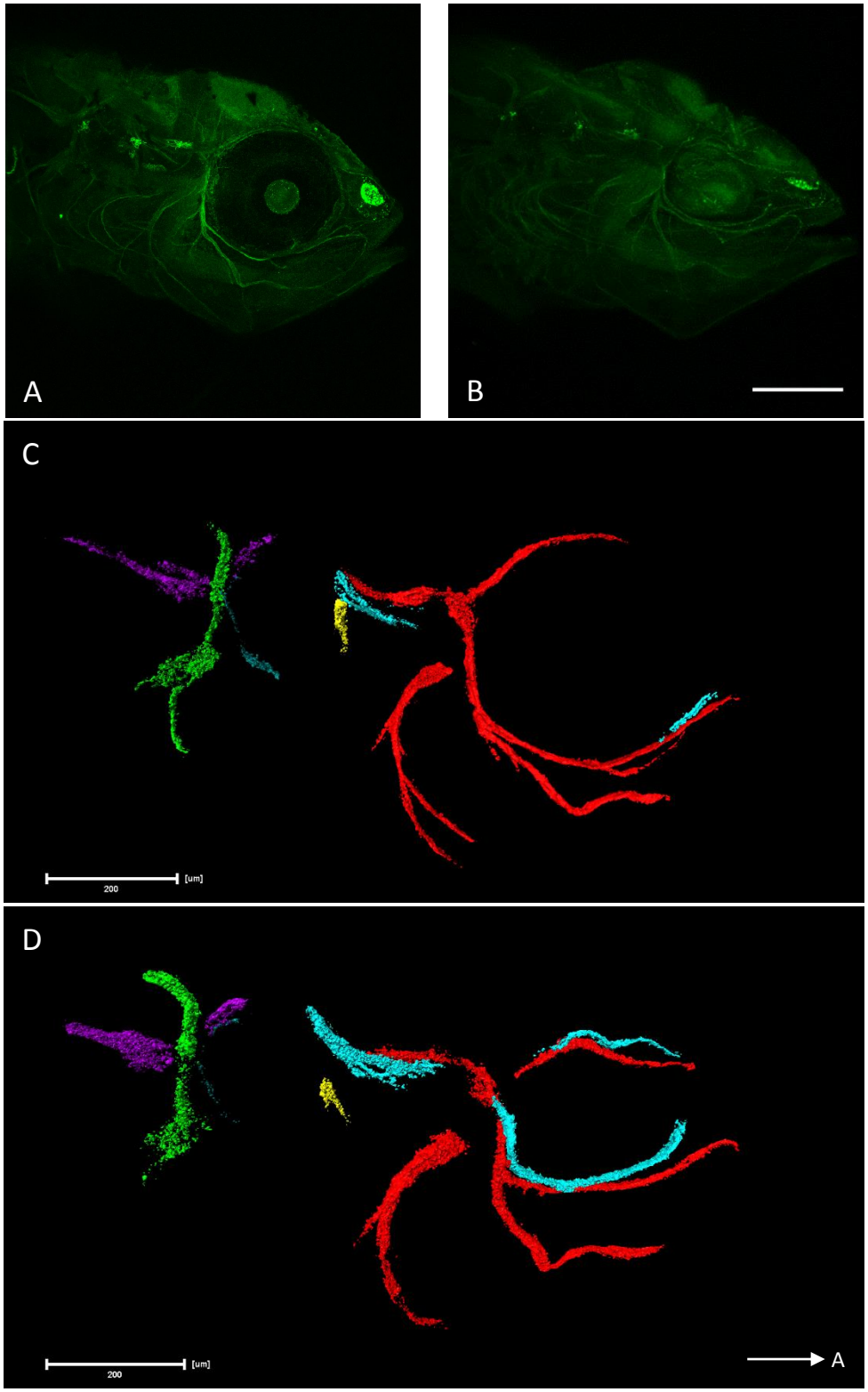

Figure 6 – CN staining and reconstruction in 5 dpf surface and Pachón cavefish. A and B show the confocal image of both surface (A) and cavefish (B) stained for Aαt. All images show the right lateral side and the arrow in the right bottom corner indicates the anterior direction. The difference in eye size at this stage is visible. As mentioned, the signal is not quite strong but allows visualization of the nerves. From these images, reconstructions were made in Amira. C shows the CN reconstruction of a surface fish and D the cavefish. Both images share the same colour code: CNV in red; ALLN in light blue; CNVIII in yellow; CNIX in ocean blue; PLLN in purple and CNX in green. Note the patchy aspect of CNX and PLLN (scale bars at 200 µm).

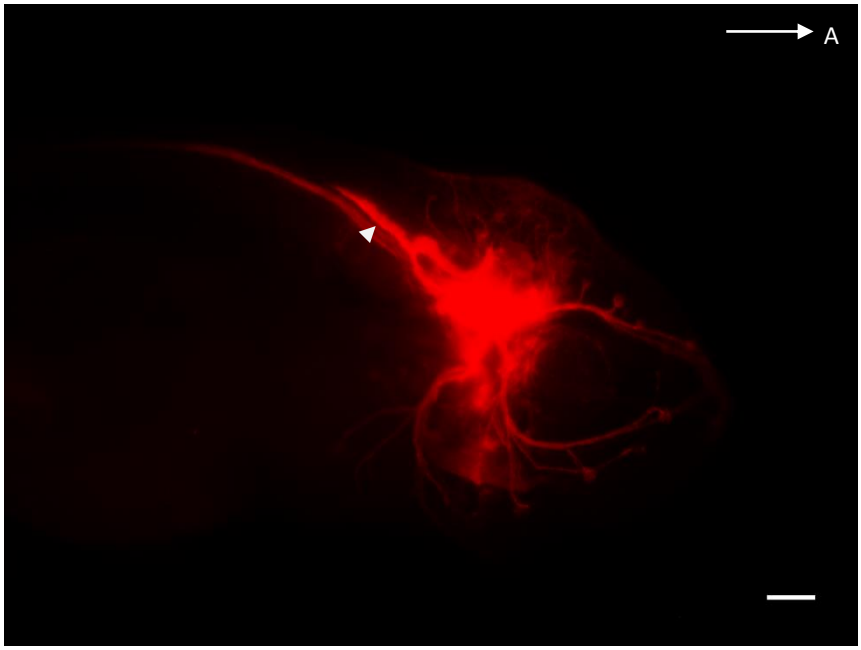

Figure 7 – DiI injection to the Anterior Lateral Line Ganglion of a 5 dpf Pachón. The arrow in the right top corner indicates the anterior direction. This injection not only labelled the anterior branches of the ALLN, but also labelled parts of the trigeminal. The lateral line neuropil in the hindbrain is also visible (arrow) (scale bar, 200 µm).

Adult cranial nerve reconstruction and measurements

Adult cranial nerves were reconstructed from micro-CT scans of PTA stained fish. Reconstructed micro-CT files were loaded into Amira 5.3.3 and all the nerves reconstructed. The differences in anatomical complexity between the virtual sections of surface and Pachón fish did not allow identical nerve reconstructions. This is most evident for the ALLN and CNV. Based on previous reports in fish [56-58], CN neuroanatomical distribution was inferred. Due to the lack of detail, some of these nerves were not identified properly, namely CNVII, CNIX and CNX. The hypothetical IX and X nerves were reconstructed (Fig.8) but not measured. These two were distinguished from the PLLN because the latter could be traced to the trunk's lateral midline.

The 3D images obtained from both surface (n=4) and Pachón cavefish (n=4) (Fig.8 and 9) were sectioned and the nerves' robustness measured. After normalization with the fishes' surface area, the values were compared using the appropriate tests. After confirming all normality and homoscedasticity assumptions (Shapiro-Wilk tests $p>0.05$, Cochran C Test $p>0.05$), an ANOVA test was used to compare the two morphotypes except for the CNII. Post-hoc analysis were done using Scheffé's test. The results, as shown in the boxplots, show significant differences in vision related nerves, the trigeminal and the ALLN (Fig.10 and 11). The CNII shows the expected reduction in cave morphotype (Mann-Whitney U, $p=0.03$), along with the CNIII (ANOVA, $p=0.008$) and the CNIV ($p<0.001$) (Fig.10). Both the trigeminal and ALLN show significant increases in their robustness in the cavefish ($p<0.001$ and $p=0.002$, respectively) (Fig.11). The olfactory (Fig.10), octavolateral and PLL (Fig.11) nerves did not show differences between the two morphotypes.

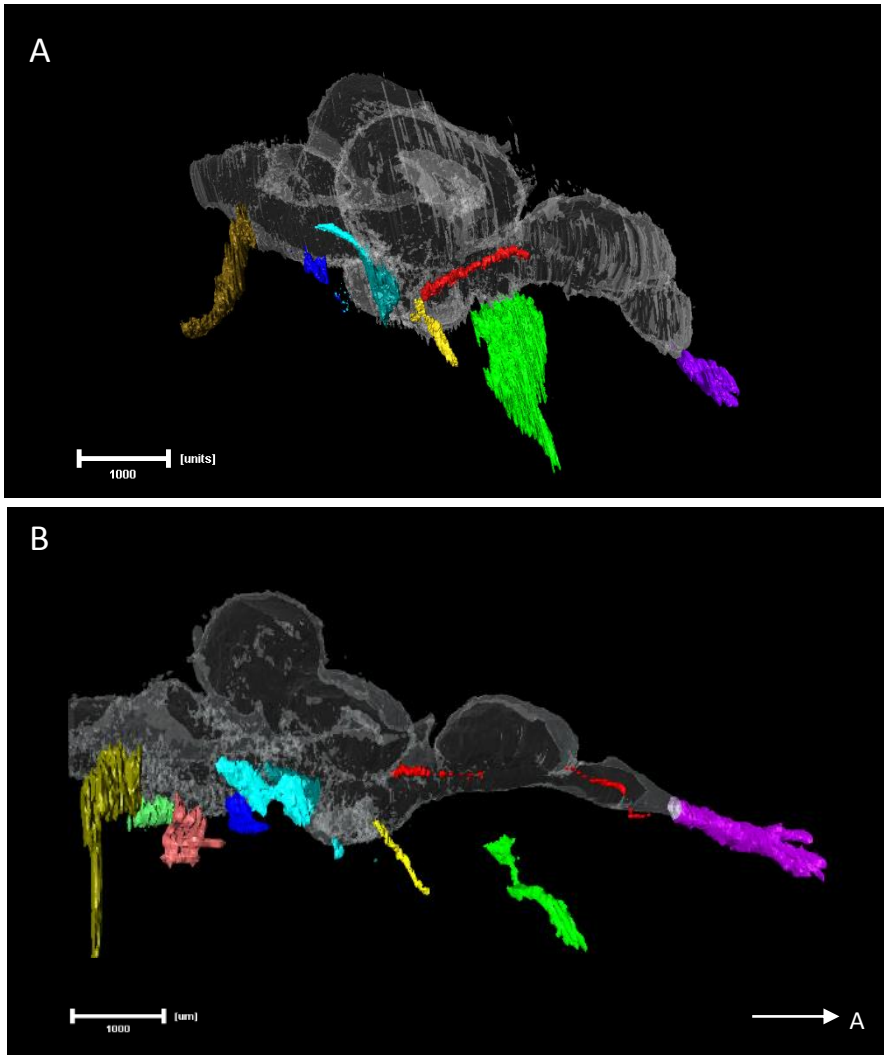

Figure 8 – Right lateral views of Amira 3D reconstructions of the CNs and brain of both adult surface fish (A) and Pachón cavefish (B). To better understand their position, a brain reconstruction was also added to the image (white transparent). The arrow in the right bottom corner indicates the anterior direction. All measured nerves share the same colour code, from anterior to posterior: CNI in purple; CNII in green; Oculomotor in yellow; Trochlear in red; ALLN in light blue (arrow); trigeminal in ocean blue, close to the ALLN; CNVIII in dark blue and PLLN (the most posterior) in a shade of green. The hypothetical CNIX and CNX were reconstructed in the cavefish (in light red and green, respectively) (scale bar set to 1 mm).

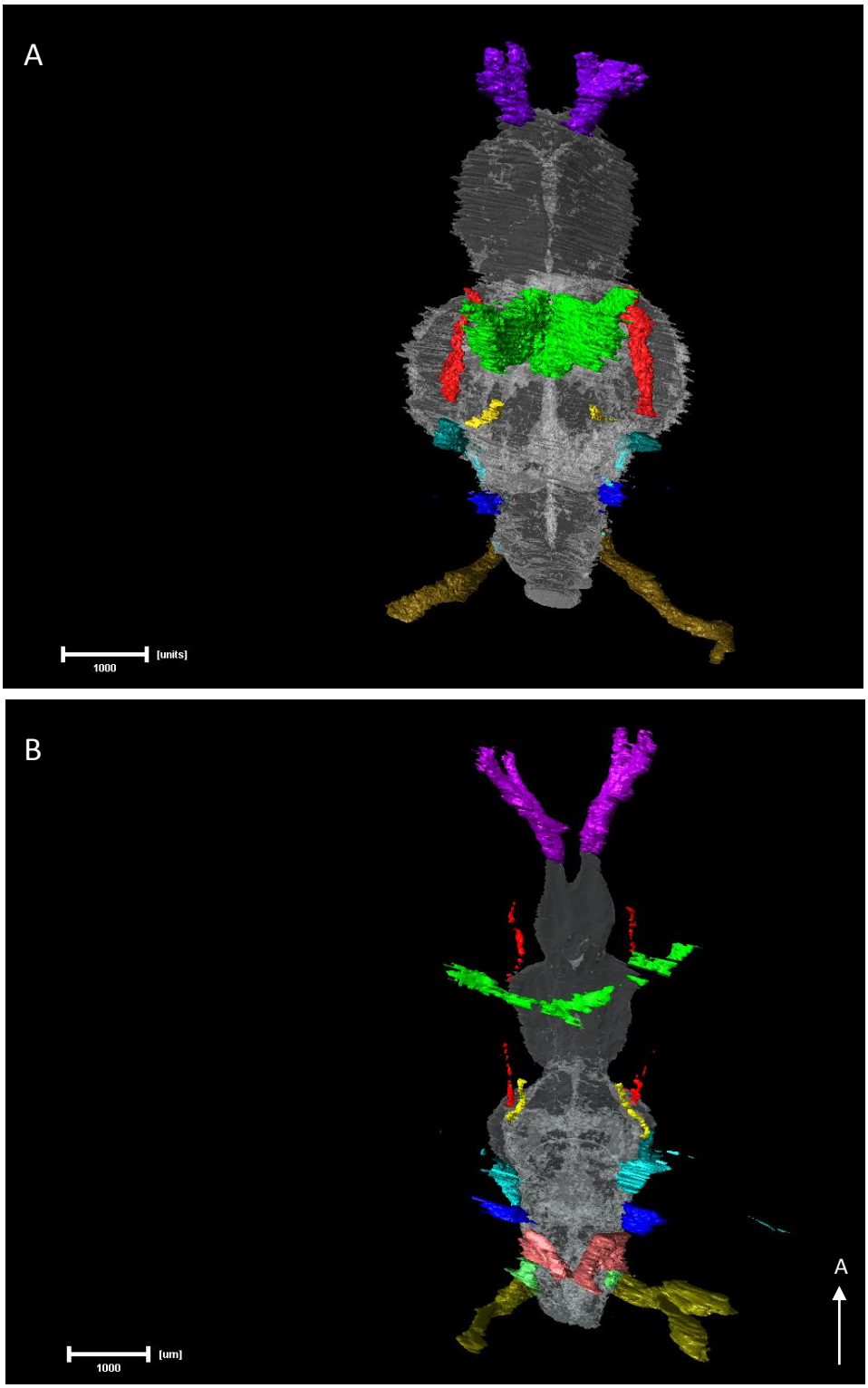

Figure 9 – Dorsal views of Amira 3D reconstructions of the CNs and brain of both adult surface fish (A) and Pachón cavefish (B). To better understand their position, a brain reconstruction was also added to the image (white transparent). The arrow in the right bottom corner indicates the anterior direction. All measured nerves share the same colour code, from anterior to posterior: CNI in purple; CNII in green; Oculomotor in yellow; Trochlear in red; ALLN in light blue (arrow); trigeminal in ocean blue, close to the ALLN; CNVIII in dark blue and PLLN (the most posterior) in a shade of green. The hypothetical CNIX and CNX were reconstructed in the cavefish (in light red and green, respectively) (scale bar set to 1 mm).

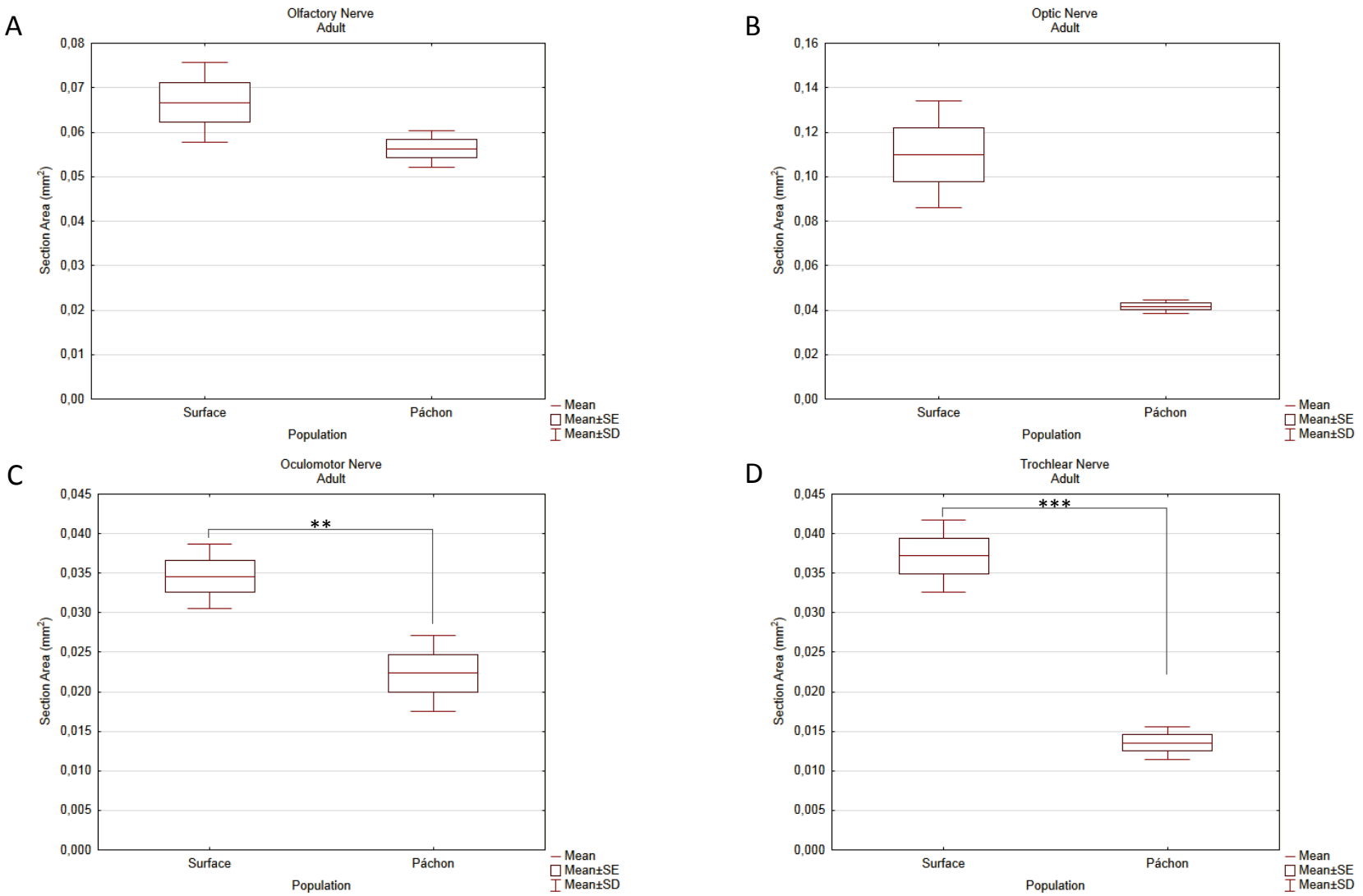

Figure 10 – Boxplot graphs showing the differences in section area of CNI (A), CNII (B) CNIII (C) and CNIV (D) between the two adult morphotypes. Boxplots were constructed using mean, standard error and standard deviation. Significance is shown where relevant (** for p<0.01; *** for p<0.001).

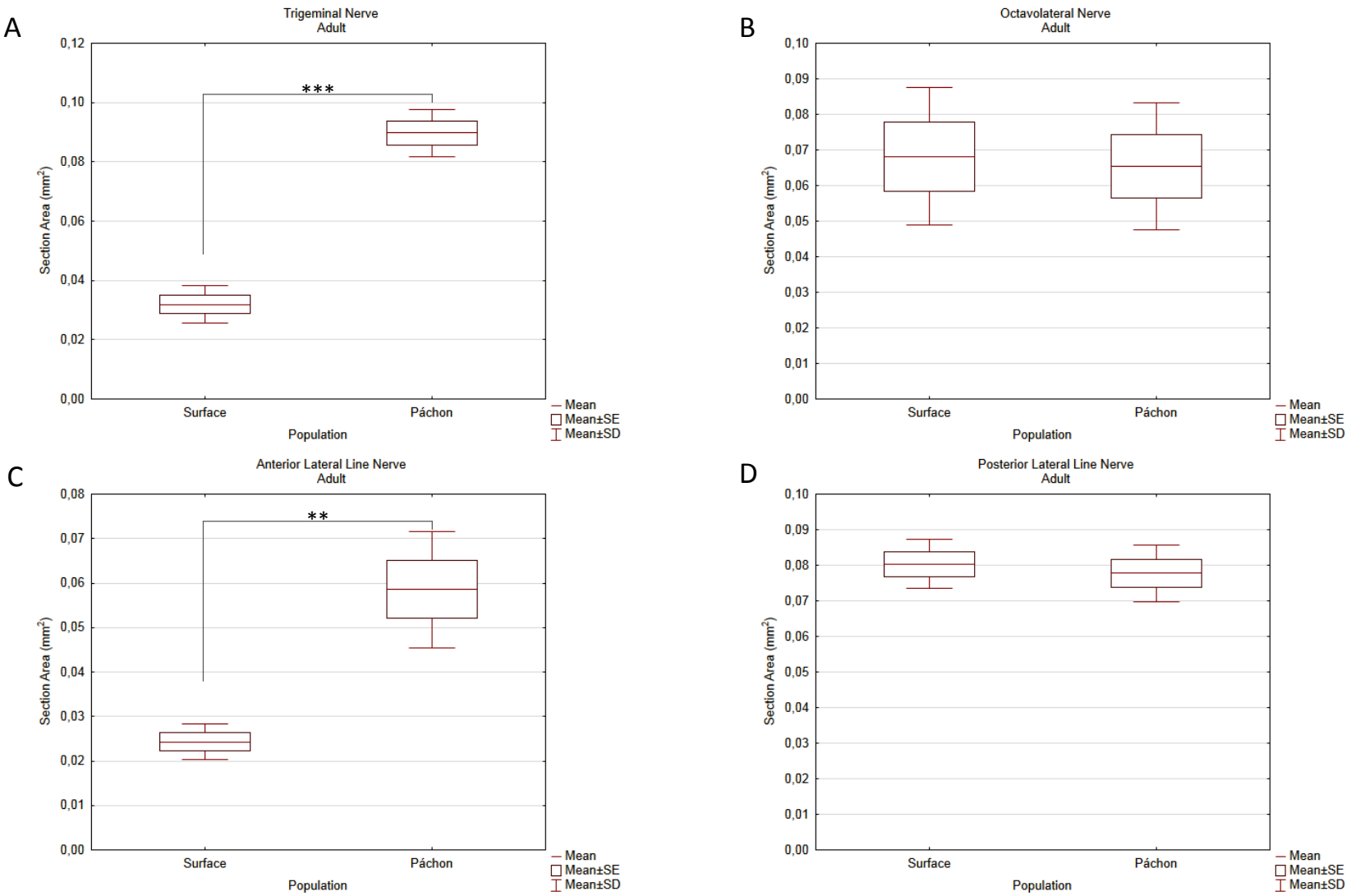

Figure 11 – Boxplot graphs showing the differences in section area of CNV (A), CNVIII (B), ALLN (C) and PLLN (D) between the two adult morphotypes. Boxplots were constructed using mean, standard error and standard deviation. Significance is shown where relevant (** for $p<0.01$; *** for $p<0.001$).

Brain morphology

Brain morphology was compared between the two morphotypes through micro-CT reconstructions of PTA stained adult and 5 dpf fish. The overall brain volume was normalized by each fish's body volume to analyse each specific stage. OB, telencephalon, TeO, hypothalamus and cerebellum were measured and compared. For each of these structures and for the brain itself, ANOVA tests were performed along with the post-hoc tests. ANOVA's assumptions were verified for all variables and except for the TeO. For this reason, tectal ratios in both stages were compared with non-parametric (Mann-Whitney U) tests.

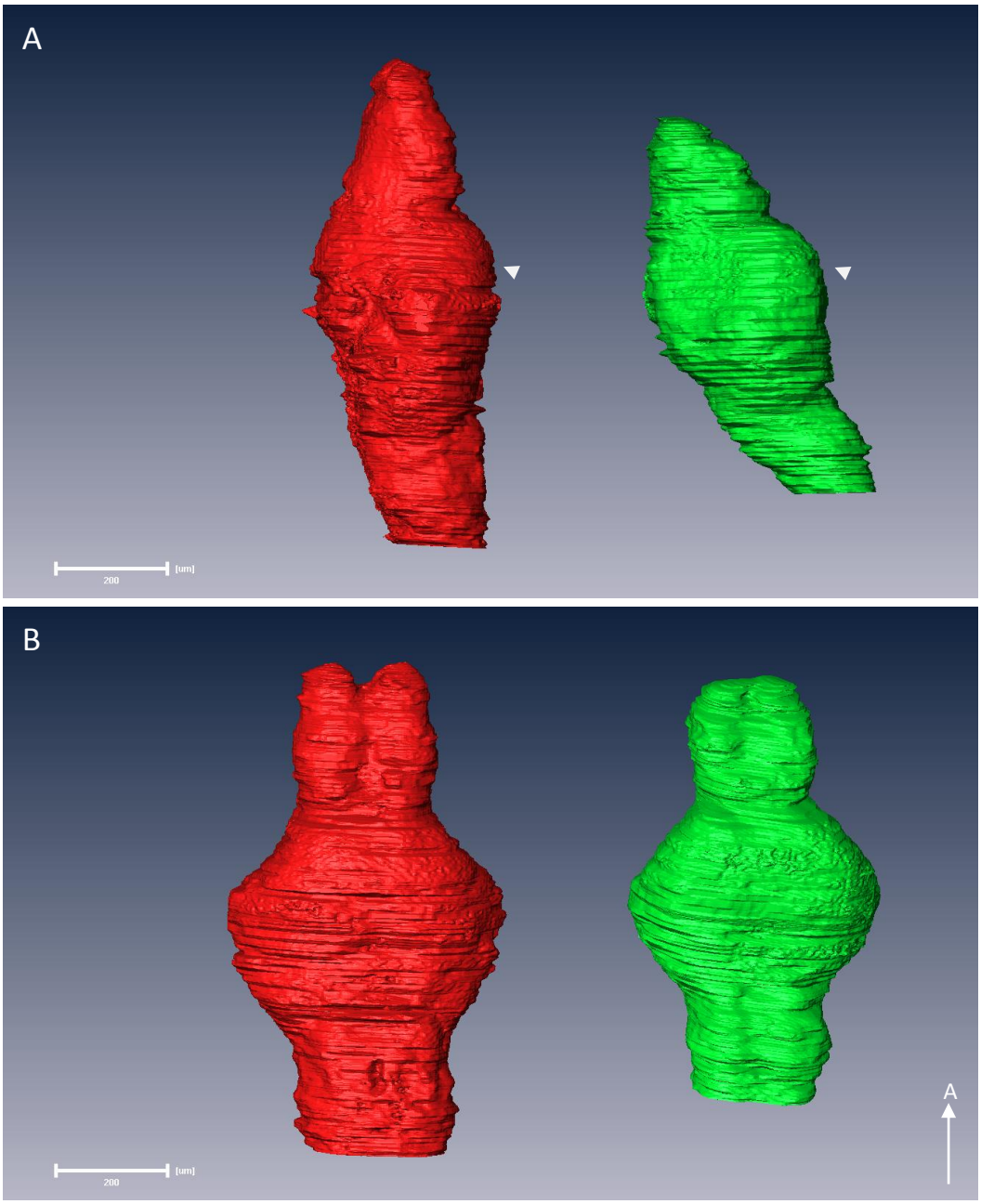

Figure 12 – Lateral (A) and dorsal (B) view of Amira reconstructions of Pachón (red) and surface (green) larval brains in 5 dpf stage. The arrow at the bottom right corner indicates the anterior direction. The arrows in figure A indicate the dorsal portion of the brain and are located just over the TeO (scale bar at 200 µm).

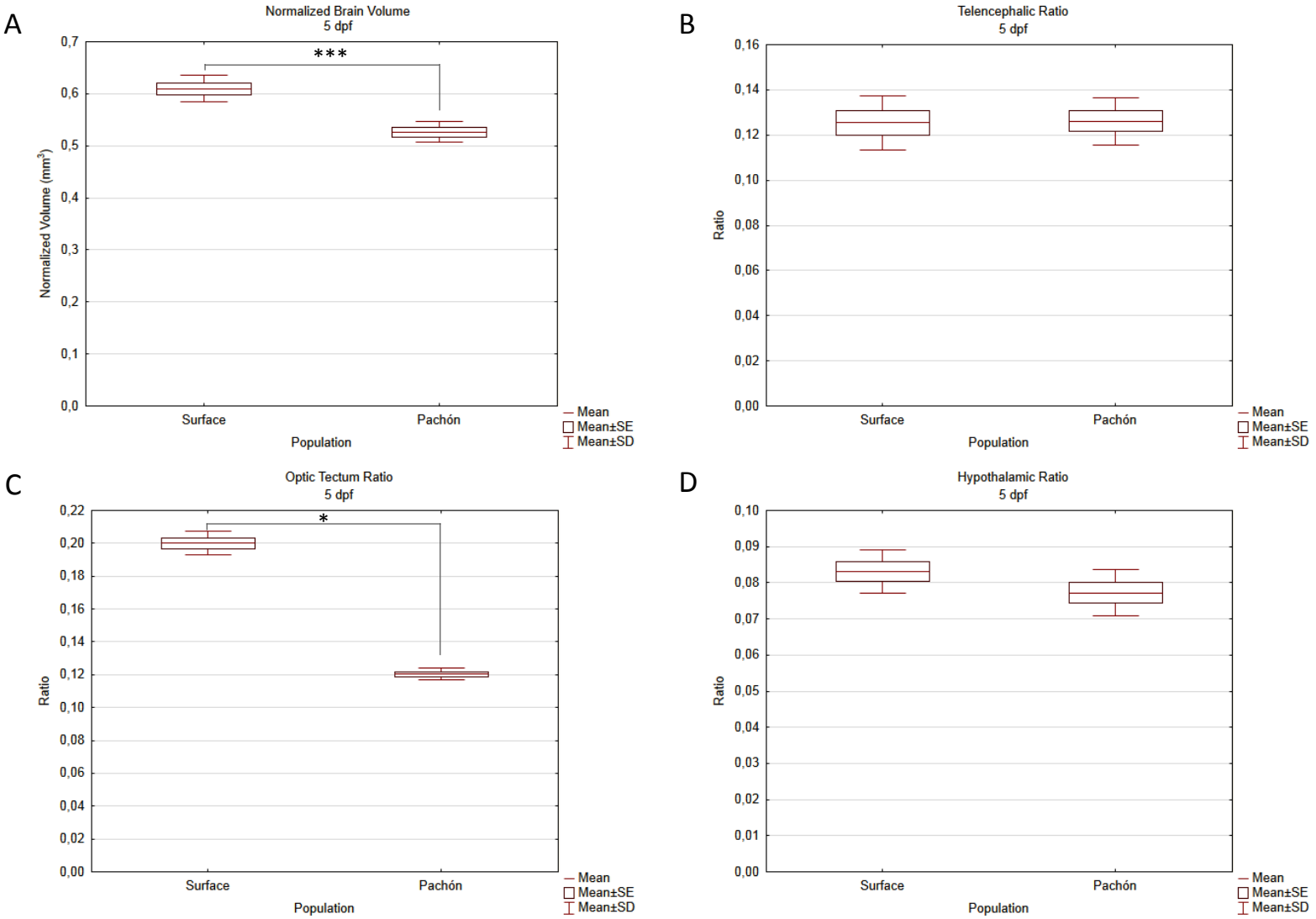

Figure 13 – Boxplot graphs showing the differences in normalized brain volume (A), and also in the telencephalic (B), tectal (C), and hypothalamic (D) ratios between the two morphotypes in the 5 dpf stage. Boxplots were constructed using mean, standard error and standard deviation. Significance is shown where relevant (* for $p<0.05$; *** for $p<0.001$).

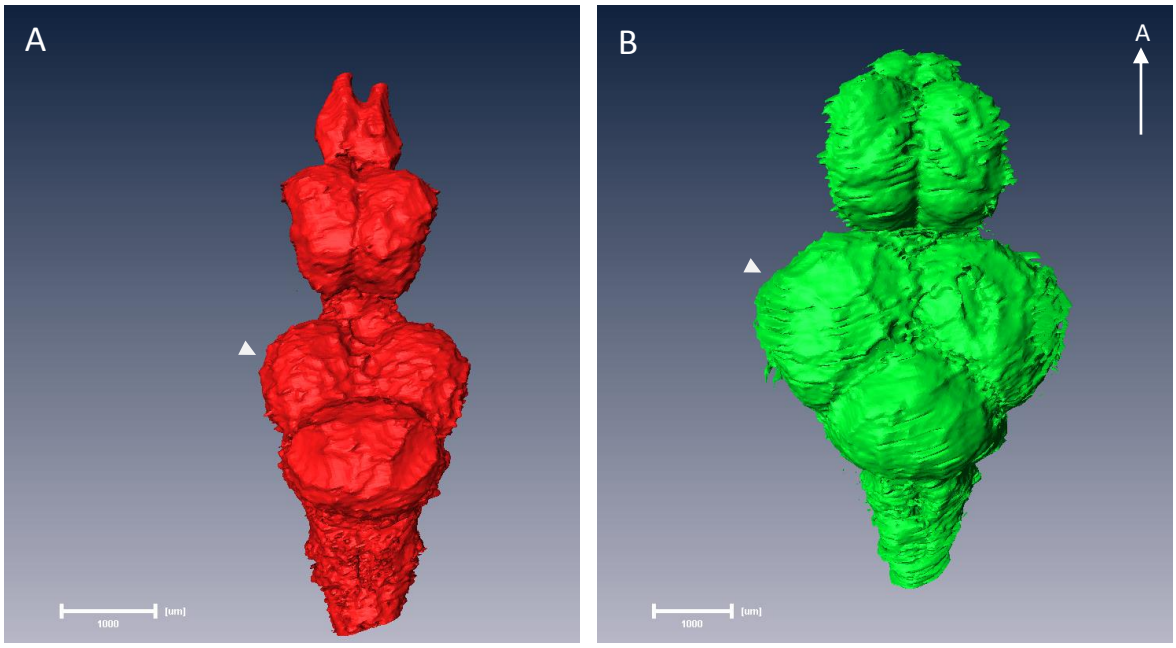

Figure 15 – Dorsal view of Amira reconstructions of Pachón (A) and surface (B) adult brains. The arrow at the top right corner indicates the anterior direction. The smaller arrows in both images indicates the TeO. The magnifications are different between the two images (scale bar at 1000 µm).

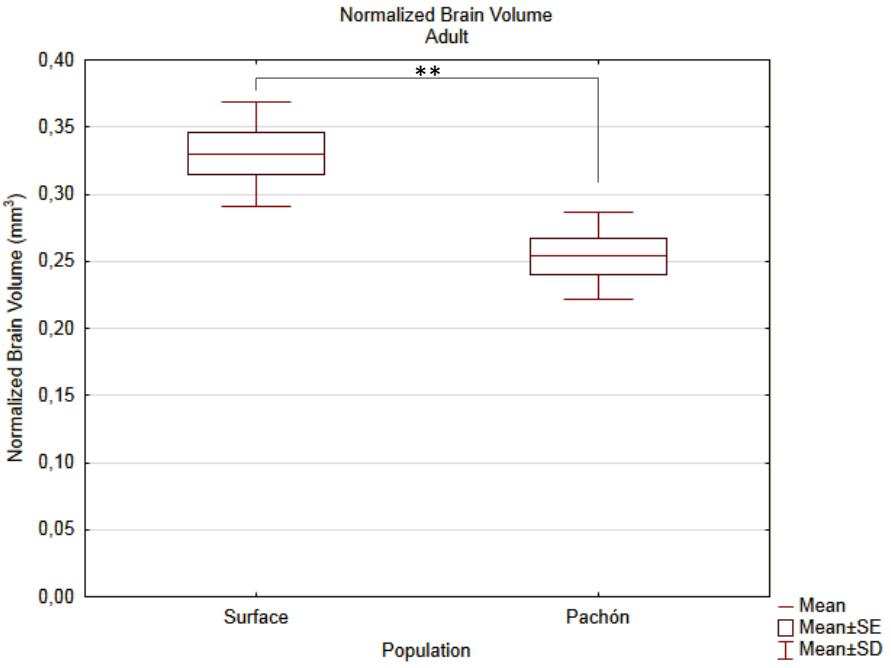

Figure 14 – Boxplot graph showing the differences in normalized brain volume between the two morphotypes in the adult stage. Boxplots were constructed using mean, standard error and standard deviation (** for $p<0.01$).

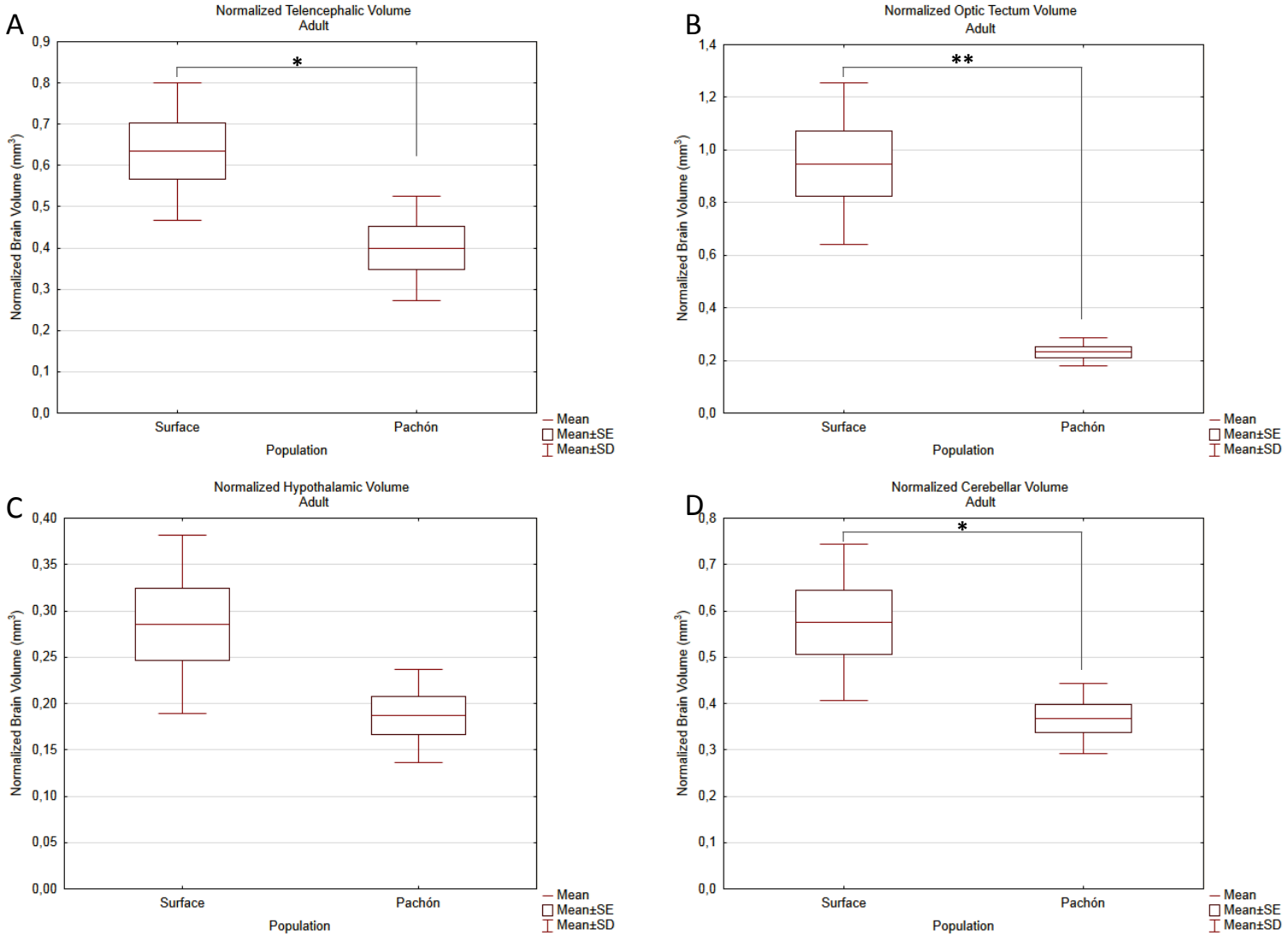

Figure 16 - Boxplot graphs showing the differences in normalized telencephalic (A), tectal (B), hypothalamic (C) and cerebellar (D) volumes between the two morphotypes in the adult stage. These values were obtained by dividing each region's volume by the overall fish volume. Boxplots were constructed using mean, standard error and standard deviation. Significance is shown where relevant (* for $p<0.05$, ** for $p<0.001$).

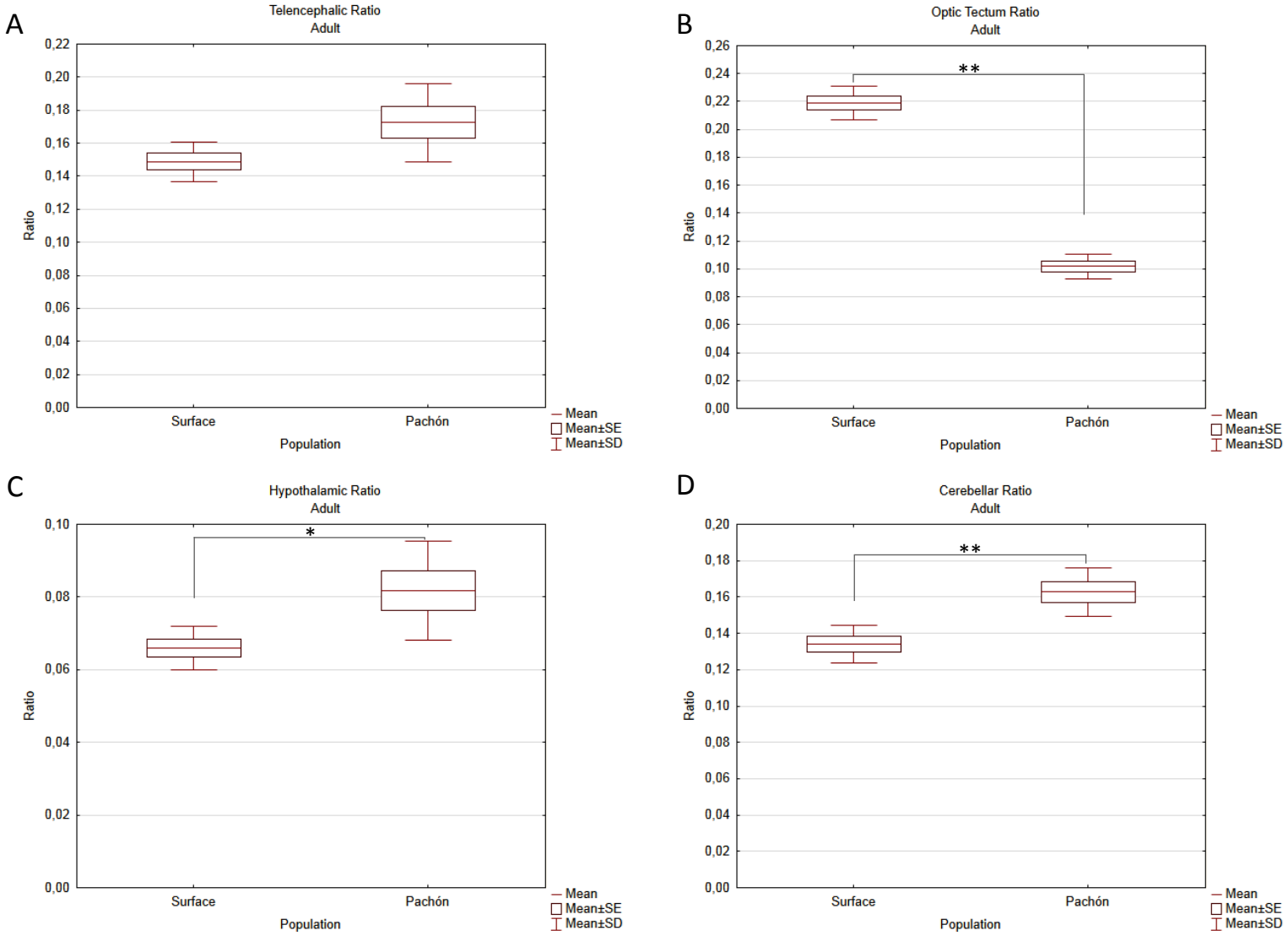

Figure 17 – Boxplot graphs showing the differences in telencephalic (A), tectal (B), hypothalamic (C) and cerebellar (D) ratios between the two morphotypes in the adult stage. Boxplots were constructed using mean, standard error and standard deviation. Significance is shown where relevant (* for $p<0.05$, ** for $p<0.01$).

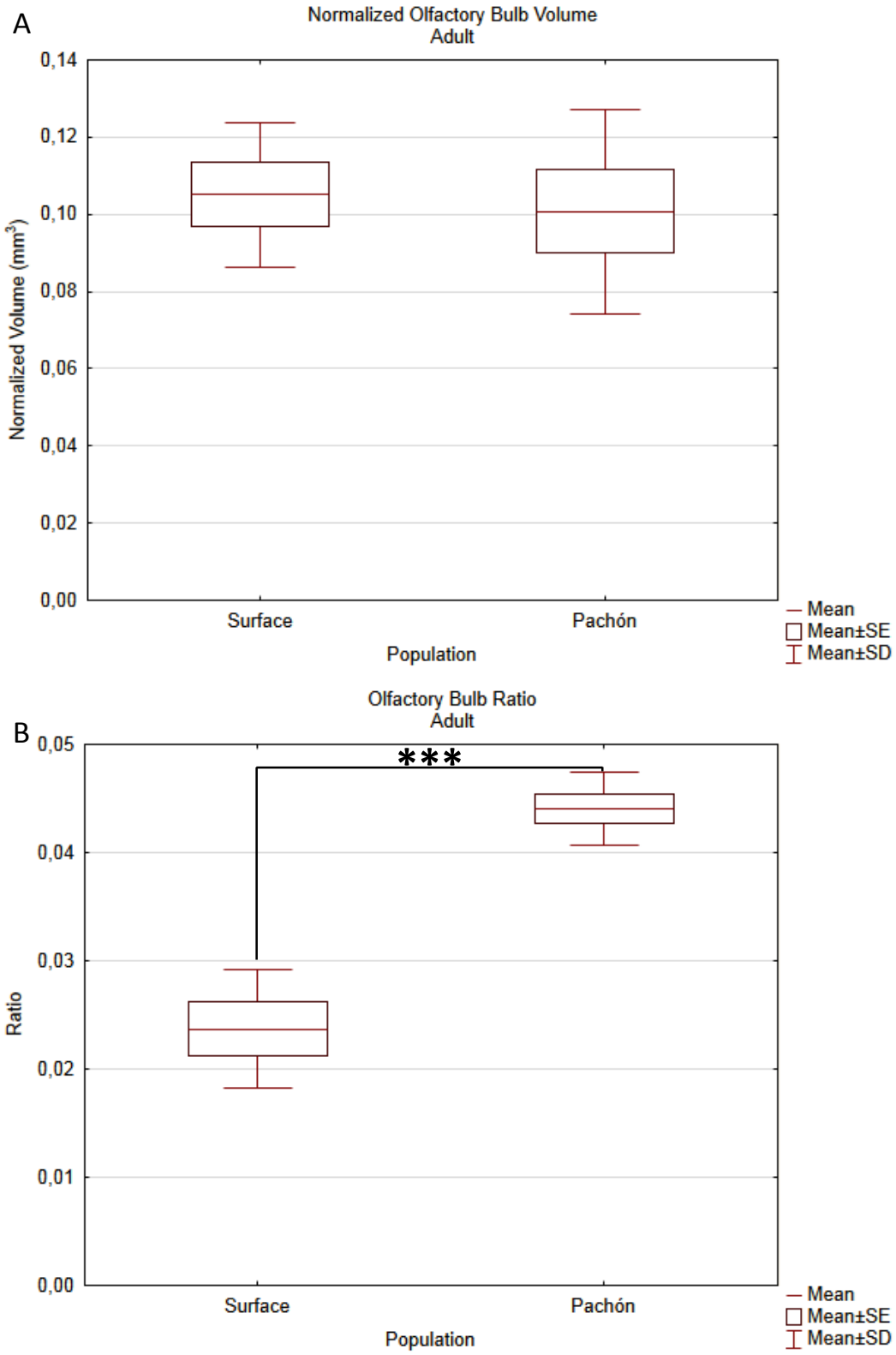

Figure 18 – Boxplot graphs showing the differences in normalized OB volume (A) and OB ratio (B) in the adult stage. Boxplots were constructed using mean, standard error and standard deviation. Significance is shown where relevant (*** for p<0.001).

The brain of the Pachón larvae (n=5) appears to be bigger than the surface fish's brain (n=5) (Fig.12), but after normalization the Pachón larval brain seems to be significantly smaller than that of the surface fish larvae (ANOVA, $p<0.001$, Fig.13 A). To further dissect possible differences, three brain regions were compared. Unlike what previous studies have implied [38, 39], neither telencephalic nor hypothalamic ratios show differences between populations at this stage (Fig.13 B and D). However, an approximate 50% reduction in the TeO is already visible in the cavefish larvae (Mann-Whitney, $p=0.01$, Fig.13 C). This is in agreement with previous reports which state that tectal differences arise early in development [42, 44]. This last result reinforces the accuracy and reliability of the method.

In the adult stage, the surface fish brain is still bigger (approximately 22%, ANOVA $p=0.004$) than the Pachón's (Fig.14 and 15). As it is visible in the reconstructions (Fig.14), the TeO is clearly less expanded in the adult cavefish. Also, the telencephalon, just anterior to the TeO, takes a cone-like shape in the Pachón (with the base and widest part at its anterior pole and the tip in its posterior one), compared to the more cylindrical shape of the surface fish's. The OBs in the cavefish seem to be slightly more elongated, but they are more bulbous in the surface fish (Fig.8 and 14).

When comparing the normalized adult volumes, the hypothalamus (Fig.16 C) and OB (Fig.18 A) show no significant differences, unlike the TeO (Mann-Whitney U, $p=0.0012$, Fig.16B), the telencephalon and cerebellum (ANOVA, both regions with $p=0.02$). Comparisons between the adult tectal ratio of both morphs show, like at 5 dpf, the same significant proportional 50% difference between both morphs (Mann-Whitney U, $p=0.005$, Fig.17 B). The Pachón's telencephalic ratio (Fig.17 A) is higher than the one of its surface counterpart, however this difference is marginally not significant (ANOVA, $p=0.054$). The hypothalamus also seems to obey the telencephalic trend, being enlarged in Pachón's brain (Fig. 17 C). This difference is, in fact, significant (ANOVA, $p=0.025$), but this structure was not easily defined through the virtual sections (ROI selections may have include some non-hypothalamic nuclei). The cavefish cerebellar ratio is also significantly higher than the surface fish's (ANOVA, $p=0.002$, Fig.17 D). The cavefish's OB also shows significant higher ratio in contrast with the surface fish's (Fig.18 B ANOVA, $p<0.001$).

To test the possibility that changes in other regions may be masked by modifications in the TeO, the telencephalic, cerebellar and hypothalamic volumes were all individually normalized by the whole brain volume without the TeO's volume. As a result, proportions of the measured regions do not differ between morphotypes (Fig.18) with the exception of the OB (ANOVA, $p<0.001$). To further confirm these results, tectal size was proportionally increased in the Pachón cavefish and its ratios recalculated. The results were the same: only the OB shows still significant differences (S.Fig.6 B ANOVA, $p<0.001$). The same measurements were made for 5 dpf fish (S.Fig.3).

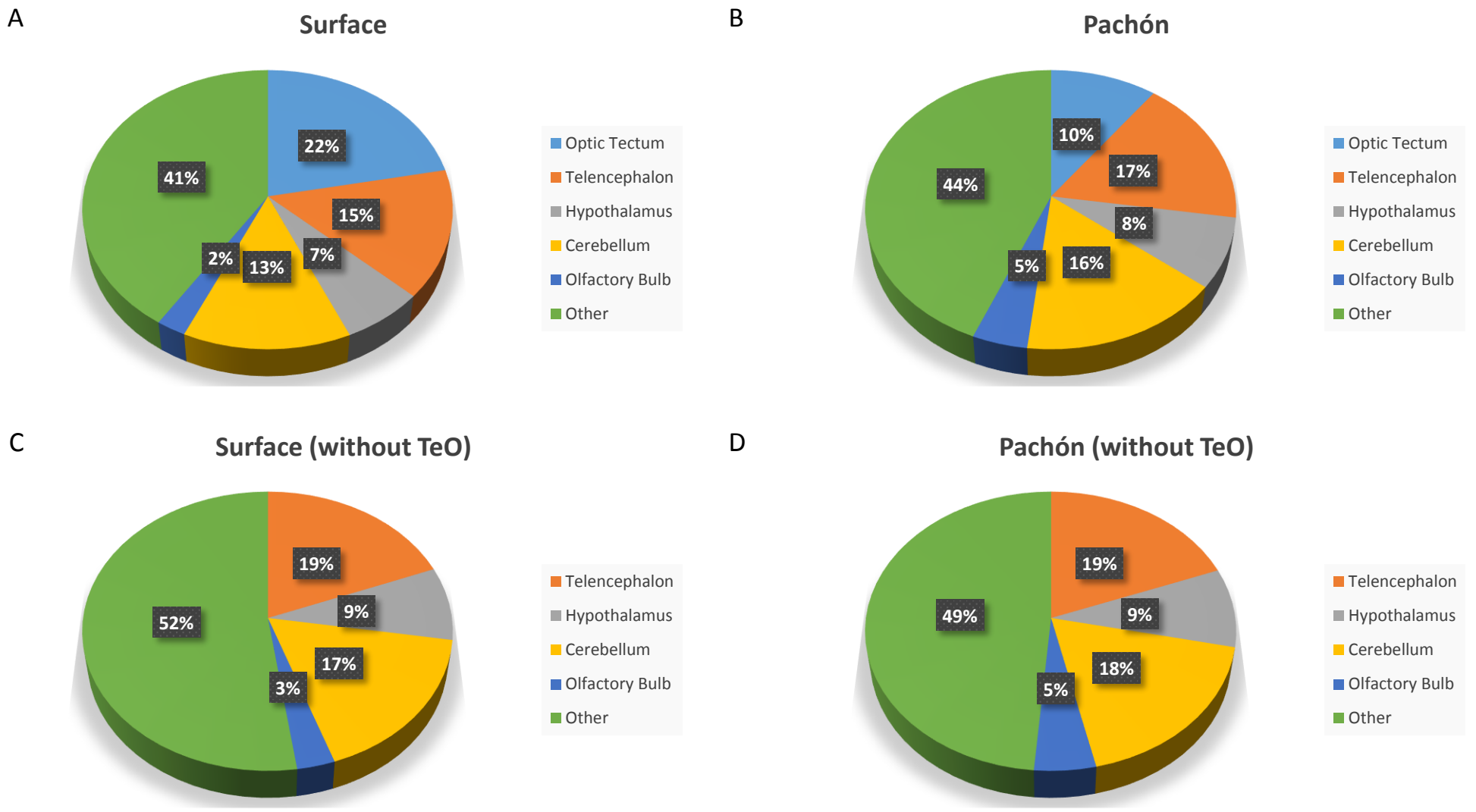

Figure 19 - Pie charts showing the different ratios of each analysed brain region in adult fish. A and B represent the mean ratios measured for each region, previously compared between both morphotypes. C and D are the mean ratios for each region calculated by excluding the tectal volume from the overall brain volume. No differences are found between both morphotypes when this ratio is measured (ANOVA, $p>0.05$) except for the OB ($p<0.001$).

Discussion

This analysis allowed to uncover: (1) significant reductions in vision related nerves accompanied by a TeO reduction in the Pachón cavefish; (2) increases in CNV and ALLN, perhaps related with enhanced sensory abilities in the cave morph; (3) the cavefish brain appears to be smaller than its surface counterpart; (4) relative expansion of the OB in the cave morphotype and (5) no differences in the telencephalon, hypothalamus and cerebellum between both populations

Methodology

The enzyme metallography staining at 5 days for Aαt would be the most interesting and accurate method to measure and compare CN. Unfortunately, the amount of silver deposits was enough for light detection, but not for x-ray detection. After several attempts, no actual solution was found for this issue. In a personal communication from Dr Brian Metscher, we were told that other labs that had tried this method with zebrafish were also unsuccessful. We thus inferred that this method would probably not work. The opportunities to optimize the method were scarce due to the lack of slots for scanning. For this reason we moved on to immunostaining in paraffin sections.

After sectioning however, portions of tissue from every other section detached from the slides. The most likely cause ought to be the lack of experience by the operator (as others have performed the same method and never experienced this problem). While staining the sections for Aαt, it was determined that the best dilution for the primary antibody was 1:50, which produced great results with alexa conjugated secondary antibodies. It is thus possible that the Aαt EnzMet™ staining did not work properly due to the fact that the primary antibody was highly diluted (1:2000). To confirm this, another Aαt EnzMet™ staining could be performed using a 1:50 dilution for the primary antibody and secondary HRP-conjugated antibody at 1:200. This could increase the amount of silver agglomerates in the nerves and create enough x-ray contrast to image them. The OPT was another possible alternative, but due to time constraints and to the faulty apparatus, we could not proceed with this method.

It was also possible to use PTA stained 5 dpf samples to reconstruct the CNs, but these were often difficult to find. Due to their small calibre, their tracts were also mistaken with other structures. Nevertheless, some of them were actually reconstructed, namely the CNII and the PLLN.

For the confocal imaging, the primary antibody dilution used was 1:200. This dilution proved not to be enough to get excellent images. As this method was used at the last minute, it was not possible to start another staining and image the samples again.

Vision related nerves

To determine changes in the degree of neural input, each CN's section area was measured at a specific point. The measurements of the CNs yielded significant decreases in the robustness of the optic and eye muscle nerves in cavefish. This is the first time optic muscle innervation in *Astyanax* has been looked at in close detail. Their large width in surface fish made it easy to trace them from their target muscles into the brain. In the Pachón however, these were much smaller, making their reconstruction more difficult. Nevertheless, the adult cavefish, even with a degenerated eye, still retain these nerves and their respective muscles, though they seem atrophied like the CNII. At post-natal stages, there is an important bidirectional cross-talk

between muscle development and its innervation [61]. Due to eye degeneration in the cavefish, the muscles may have become increasingly disorganised and their lack of stimulation may have driven the hypotrophy of these nerves. On the other hand, changes in the nerves' nuclei may have already reduced their section area, which in turn also cause eye muscle atrophy. Coordinated modifications on both ends may also have happened. A closer look at the CNs at 5 dpf and at the muscle structure would provide more information about the coordinated modification these structures. The micro-CT data gathered could be used for this purpose – measuring the overall volume of these muscles at different stages and comparing them between morphotypes.

The Abducens nerve, which innervates the lateral rectus muscle, was not properly reconstructed. Due to its small calibre it was not easily tracked. It was actually reconstructed in a few surface fish (2 out of 4), but not once in the Pachón.

The CNII's robustness in both stages confirms previous reports about its reduction in the cavefish [42, 44, 47]. This reduction is associated with the lens degeneration in the hypogean morphotype. This causes a reduction in the number of ganglion cells which project axons towards the tectum [47, 51]. By transplanting a surface fish lens into a cavefish, this phenotype is partially rescued, allowing an increase in both ganglion cell number and optic nerve width [47]. Its impact on the cavefish's TeO development is more controversial, but it will be discussed further ahead.

Olfactory and Octavolateral nerves

The CNI shows no differences in section area between both morphotypes. This is agreement with a previous report states that despite the idea that olfaction should be an enhanced in the cavefish, the OB is quite similar to other teleosts in its nuclear organisation [35]. However, there might be important qualitative modifications in the Pachón's olfaction which do not reflect in the amount of axons going into the brain. This last idea is reinforced if we consider the likely enhancement of the cavefish OB (discussed ahead).

The octavolateral nerve also shows no differences between both morphotypes. This is in agreement with previous reports which suggest that, even though these fish respond to a wider range of sound frequencies, there are no differences between both morphotypes [34].

Trigeminal and Lateral Line modifications

An overall increase in trigeminal and ALLN width was detected in the adult cavefish. The trigeminal nerve is responsible for conveying information about "general senses", namely: head somatosensory information, position, pain and temperature. The trigeminal's motor component is responsible for jaw muscle innervation [10]. Considering these aspects, both sensory and motor functions of the CNV could be enhanced in the Pachón.

It has been suggested that the cavefish's somatosensory abilities are enhanced in comparison to its epigean relatives [41]. This increased short-range sensibility elicits new behaviours in his morphotype, like "wall following behaviour", allowing environmental exploration through touch [41, 62]. Hence, the Pachón's increase in the trigeminal width can be related to this enhanced input. This exploratory behaviour, however, requires also another enhanced sense, the LLS.

There are virtually no differences in the neuromast distribution across the trunk of the fish between morphotypes [63]. This is in agreement with the measurements made for the PLLN, which show no differences between the populations. In the cavefish's head region however,

paralleling the loss of the eye, significant increases in the number of neuromasts have been reported [27, 49, 50, 63]. Moreover, these are also structurally modified, allowing a heightened sensitivity [28, 29]. The larger section area of the cavefish's ALLN correlates very well with these modifications. With this boosted mechanoreception, the LLS detects objects at a wider range through the distortion of the water motion created by the fish's swimming movements. This ability, complemented by the enhanced somatosensory input, allows the fish to create a mental representation of their environment, a process termed hydrodynamic imaging [28-30, 62, 64]. Improving senses that allow habitat exploration in a "dark" environment is necessary to compensate for the lack of customary vision-based navigation [11]. Thus, somato- and mechanoreceptive enhancement seems indispensable for cavefish, for it creates a non-visual navigational system that allows these populations to thrive in absence of light.

The reconstructions made through Amira may not solely represent each CN. For instance, the facial nerve runs along with the trigeminal [58] and, like the glossopharyngeal and vagus nerves, is responsible for directing taste information to the brain. Given the increase in TB number in the cavefish, it is also likely that their section area is also increased. Nevertheless, the fact that the nerves were measured closer to the brain decreases the chance of misidentifying them.

Changes in brain shape and morphology

Surface fish have a significantly larger brain compared to cavefish. This decrease in adult brain volume in the cave environment may be related to energy consumption. Exchanging neural information has high metabolic cost (around 20% in humans) [65]. Also, recent experiments have shown that selection for bigger sized brains entails trade-offs with reproductive abilities and gut size in guppies, as individuals selected for a larger brain had less progeny and smaller guts [66]. Thus, a reduction in the overall brain seems advantageous in the cave environment, where food is scarce and oxygen levels are lower than normal. Even though it is tempting to attribute an adaptive value to this reduction, we cannot exclude the role of other evolutionary forces, like genetic drift, in the shaping of this trait. However, as other cave teleosts appear to share the same phenotype [67], this reduction may be important in such environment.

The most striking morphological difference detected, besides the TeO, was in the telencephalon. It is important to note that previous reports have stated that there are no significant telencephalic changes in the cavefish [36]. These works were done in strains of commercial cavefish which, as it is known, have crossed often with surface fish and were artificially kept for generations in aquariums as pets, meaning that these results may not represent the cave phenotype. A description of these differences in other cavefish population might give a more accurate view on telencephalon modifications.

The Tectum and Olfactory Bulb

Tectal differences were as expected: approximately 50% reduction of the overall tectal size in cavefish in comparison to surface fish in both stages [42, 44, 47]. These tectal differences seem to arise due to a hypoplasia derived from the lack of innervation from the optic nerve. There is, in fact, a significant (approximately) 60% reduction in the CNII robustness in the adult Pachón. The cavefish tectal reduction is already evident at 5 dpf and, as previously suggested [44], it is at this stage that the CNII reaches the TeO and begins its activity – coinciding with the stage when larvae start seeking food due to the depletion of maternal yolk. As such, this hypothetical hypoplasia may not be caused by the lack of optic innervation but it can be a fixed trait in these fish. This is reinforced by the fact that cavefish with restored eye size and function do not fully develop a surface fish-like TeO. Also, the eye/lens deleted surface individuals do not have the

same degree of tectal atrophy as their hypogean counterparts. These differences have been justified by the different number of retinal ganglion cells in the eye of both morphotypes [47]. However, the presence of tectal hypoplasia at such early stages and the lack of complete phenotypic rescue with lens transplantation/deletion in cave-/surface fish, respectively, suggests that this reduction may be a fixed cavefish trait. This is reinforced by studies that suggest that even cavefish with induced eyes do not respond to light stimuli [68]. The TeO's function in the Pachón may, thus, no longer be dominated by visual stimuli but rather by somatosensory input. Voneida et al. [41] have not only found that the cavefish TeO has a well-defined somatotopic map, but also that somatosensory stimuli seems to have taken over the TeO. The TeO's "hypoplasia" may thus be a natural and necessary state of this morphotype.

The OB, as it implies, is involved in the reception of olfactory input, which is then relayed to the telencephalic lobes. As a result, this region maps the chemosensory stimuli received at the olfactory pit [69]. Our analysis suggests an increase in this region's volume, which subsists even when the TeO's volume is excluded from the analysis. Previous works suggest that this sense is not particularly enhanced [35], which seems adequate since no actual differences in volume were found between both morphotypes. However, it is unlikely that the rest of the brain could have undergone decreases in volume while the OB remained unmodified. Also, as there is an increased number of GABA-ergic interneurons that migrate to the OB, it is more likely that this region is, in fact, enhanced in the cavefish [38]. A functional assessment of this sense may shed some light on the adaptive value of such modifications.

The case of the Telencephalon, Hypothalamus and Cerebellum

Previous works have suggested an overall larger telencephalon in the cavefish [38, 39]. We found that the overall telencephalic volume is actually smaller in the cavefish. In fish, the telencephalon is involved in cognition, learning and memory, allowing fish to develop complex social behaviours and cope with rich environments [5, 10, 11, 70]. The calculated ratios pointed for a slightly enhanced telencephalon. But, unlike what happened with the OB ratio, excluding the TeO from the brain volume yielded no significant differences between surface and cavefish.

Previous works have also shown that, during cavefish development, there is more proliferation in the hypothalamic region than in a surface embryo in the same stage due to the expansion of the ventral *shh* from the anterior midline [38]. We found, similarly to the telencephalon, that the hypothalamus is actually smaller in the cavefish. Even though the actual ratio appeared to be higher in this morphotype, excluding the TeO from the overall brain volume or when equalizing it between morphotypes eliminates these proportional differences. This suggests that these Pachón regions may just be scaled-down from surface-fish brain. Even though these increases have been suggested when analysing early development [38], it seems that they do not significantly change the adult stage. Another work has shown an increase in the serotonergic paraventricular nucleus in the cavefish hypothalamus. This caused a shift from the surface fish's aggressive behaviour to the foraging behaviour exhibited by cavefish [71]. Combining this information with the data gathered by our project, it appears that perhaps crucial CNS modifications may occur at another level of organization – in the brain's nuclei.

Increased cerebellar volume occurs in fish with increased mechanosensory/electrosensory input [10, 11]. Thus, a relative increase in cavefish cerebellar volume would be expected as a coordinated response to the enhanced LLS and somatosensory input, affecting this morphotype's spatial cognition and motor coordination [72]. Such relative increase in the cavefish, similarly to the telencephalic and hypothalamic case, does not seem to exist after we exclude the TeO from the analysis.

So, even though it appears that there has been a relative increase in particular types of sensory input in the cavefish, some of the associated brain regions have changed as expected. This either means that there is a stronger constrain that keeps this "relative hypertrophy" from revealing itself, or that the modifications are located elsewhere – in another region or at another organisational level.

Regarding the TeO's exclusion for ratio re-calculation, it is important to note that this method may not hold true if the tectal modifications are already built into the organism's genome.

On the origin of CNS differences

Early in vertebrate development, the neural plate is regionalized through the formation of its "neuraxes" [5]. Wnt antagonists and Fibroblast Growth Factors (FGFs) are secreted from the most anterior neural organiser, the Anterior Neural Ridge (ANR), committing the most anterior cells to an "anterior fate". Simultaneously, Wnt signalling from a more posterior region of the neural plate defines the other end of the Anterior-Posterior axis, thus creating the Midbrain-Hindbrain Boundary (MHB). The anti-Wnt signalling at the ANR induces the formation of the prosencephalon and, the MHB defines rhombencephalon (posteriorly) and midbrain (anteriorly) [1]. As this axis is under development, Hedgehog signals from the ventrally located notochord confer ventral identity to the neural plate, while the surrounding ectoderm defines the dorsal identity through BMP activity, thus estabilishing the Dorsal-Ventral neuraxis [1]. The concerted activity of the signals from both axes drives the formation of another organiser, the *shh*-positive zona limitans intrathalamica (ZLI).

Afterwards, these signals start acting in a more localized fashion, subdividing these vesicles into specific regions: the ANR defines rostral brain regions (telencephalon and OB); the ZLI medial regions and the MHB posterior ones (cerebellum and hindbrain). Following this process, neurogenesis takes place. Neurogenesis occurs in the Ventricular and Subventricular Zones (VZ, SVZ, respectively) of the brain and influences the growth of each region. Neural precursors are influenced by the same cues as the ones mentioned above: FGF and Wnt signalling control the number of symmetric divisions that the neural precursors undergo. When the strength of Wnt and FGF signalling decreases, neural progenitors start dividing asymmetrically, giving rise to post-mitotic neurons which migrate into the neural tissue [2-6, 73-76]. Consequently, expansion of specific brain regions is achieved by increasing the number of symmetric divisions of the progenitors (1^{st} step), whereas the asymmetric divisions (2^{nd} step) only affect neural commitment and differentiation [2, 3, 6].

Changes in neurogenesis are traditionally considered to be the cause of brain volume variations. Recent works in cichlids have shown that brain changes may also occur during brain patterning. Adult sand-dwelling cichlids seem to have a smaller telencephalon compared to rock-dwelling ones [7]. Treating embryos of rock-dwelling fish with LiCl (which enhances Wnt signalling) results in an expression patter similar to the sand-dwelling fish embryos [7].

Given what we know about *shh* expansion in the cavefish embryo, modifications in neural organisers – similar to those of the cichlids – are also likely to have occurred. The expansion of ventral *shh* could have significantly affected the brain, not just in terms of patterning but at the neurogenesis level - as seen in the cavefish's paraventricular nucleus [38]. Considering the probable modifications in telencephalon and the OB enhancement, modifications in the ANR and/or MHB could have occurred as well. Earlier changes could have also reduced the overall brain volume by changing the number of cells that commit to neural fate. Neurogenic modifications could have also significantly influenced n the proportional differences in brain regions but also the overall volume of the brain. Perhaps a combination of smaller and fewer cells could contribute to the verified decrease in brain size.

Regarding the TeO, modifications at the neurogenesis step could limit the expansion of this structure. The previously described higher number of hypothetically undifferentiated neurons in the VZ of the cavefish tectum [42] endorses this idea. Nevertheless, changes in early patterning of this region may have also affected the final tectal morphology. The lesser number of asymmetrical divisions may also be caused, as argued before, by the lack of innervation, even though this difference is present early on.

This study unveiled the presence of an "Optic Module", whereby eye, optic nerve, TeO, optic muscle nerves and the muscles themselves change as a whole and are still maintained in cavefish. This can be taken as an example of developmental constraints, as the entire optic module is developed properly in Pachón embryo but is kept as a hypotrophied non-functional module in the adult.

CNS evolution in Astyanax

This study shows independent modifications of different brain regions in *Astyanax*. This is in agreement with the Mosaic Brain Evolution hypothesis: optic related centres in the cavefish have suffered reductions as visual organs have degenerated; relative expansion of the OB in the cavefish, perhaps related to modifications in the chemosensory ability. The telencephalon, hypothalamus and cerebellum appear to be scaled-down from the ancestral, as precluding the tectum from the analysis dismisses the differences found between morphotypes. This may also indicate a negative correlation between tectal volume and the relative expansion of other brain regions, in which case, arresting the TeO's development early on would allow other brain areas to change in an orchestrated manner with sensory input modifications.

It is legitimate to assume that energetic constraints may have taken a toll in overall size and morphology of the cavefish brain, explaining its reduced volume. Constructive traits in cavefish may, thus, be evident at the CNS nuclear level and are not reflected on the overall volume of brain regions. This would explain the lack of correlation between the increased ALLN and CNV and the analysed brain regions. Perhaps other areas contain the nuclei that responded accordingly with the apparently enhanced sensory information. Determining changes in cell number, cell volume and overall brain nuclei organization may clarify some of these questions raised by this work.

On a final note, *Astyanax* cavefish show distinctive neuroanatomical features in comparison to their surface ancestors. Their divergent phenotypes, considering that speciation is still an ongoing process, demonstrate the enormous plasticity/adaptability of the CNS in response to the population's niche. It is this last feature that, ultimately, allows life to thrive even in the most unlikely places.

References

1. Gilbert SF: **Developmental Biology**, 8th edn. Sunderland, MA: Sinauer Associates; 2006.
2. Rakic P: **A small step for the cell, a giant leap for mankind: a hypothesis of neocortical expansion during evolution**. *Trends in neurosciences* 1995, **18**(9):383-388.
3. Charvet CJ, Striedter GF: **Bigger brains cycle faster before neurogenesis begins: a comparison of brain development between chickens and bobwhite quail**. *Proceedings Biological sciences / The Royal Society* 2010, **277**(1699):3469-3475.
4. Borrell V, Reillo I: **Emerging roles of neural stem cells in cerebral cortex development and evolution**. *Developmental neurobiology* 2012, **72**(7):955-971.
5. Sylvester JB, Pottin K, Streelman JT: **Integrated Brain Diversification along the Early Neuraxes**. *Brain, behavior and evolution* 2011, **78**(3):237-247.
6. Charvet CJ, Sandoval AL, Striedter GF: **Phylogenetic origins of early alterations in brain region proportions**. *Brain, behavior and evolution* 2010, **75**(2):104-110.
7. Sylvester JB, Rich CA, Loh YHE, van Staaden MJ, Fraser GJ, Streelman JT: **Brain diversity evolves via differences in patterning**. *Proceedings of the National Academy of Sciences of the United States of America* 2010, **107**(21):9718-9723.
8. Northcutt RG: **Understanding vertebrate brain evolution**. *Integr Comp Biol* 2002, **42**(4):743-756.
9. Northcutt RG: **Changing views of brain evolution**. *Brain research bulletin* 2001, **55**(6):663-674.
10. Butler AB, Hodos W: **Comparative vertebrate neuroanatomy - Evolution and Adaptation**, 2nd edn. Hoboken, New Jersey: John Wiley & Sons, Inc.; 2005.
11. Lisney TJ, Collin SP: **Brain morphology in large pelagic fishes: a comparison between sharks and teleosts**. *Journal of Fish Biology* 2006, **68**(2):532-554.
12. Iwaniuk AN, Dean KM, Nelson JE: **A mosaic pattern characterizes the evolution of the avian brain**. *Proceedings Biological sciences / The Royal Society* 2004, **271 Suppl 4**:S148-151.
13. Sanes DH, Reh TA, Harris WA: **Development of the Nervous System**, 3rd edn. Oxford: Academic Press; 2012.
14. Nieuwenhuys R, Donkelaar HJ, C. N: **The Central Nervous System of Vertebrates**, vol. 2, 1st edn. Berlin: Springer; 1998.
15. Jeffery WR: **Cavefish as a model system in evolutionary developmental biology**. *Developmental biology* 2001, **231**(1):1-12.
16. Hubbs CL, Innes WT: **The first known blind fish of the family characidae: a new genus from Mexico**. *Occas Pap Mus Zool Univ Mich* 1936, **342**:1-7.
17. Avise JC, Selander RK: **Evolutionary Genetics of Cave-Dwelling Fishes of the Genus Astyanax**. *Evolution* 1972, **26**(1):1-19.
18. Gross JB: **The complex origin of Astyanax cavefish**. *BMC evolutionary biology* 2012, **12**(1):105.

19. Jeffery WR: **Regressive evolution in Astyanax cavefish**. *Annual review of genetics* 2009, **43**:25-47.

20. Hausdorf B, Wilkens H, Strecker U: **Population genetic patterns revealed by microsatellite data challenge the mitochondrial DNA based taxonomy of Astyanax in Mexico (Characidae, Teleostei)**. *Molecular phylogenetics and evolution* 2011, **60**(1):89-97.

21. Strecker U, Hausdorf B, Wilkens H: **Parallel speciation in Astyanax cave fish (Teleostei) in Northern Mexico**. *Molecular phylogenetics and evolution* 2012, **62**(1):62-70.

22. Bradic M, Beerli P, Garcia-de Leon FJ, Esquivel-Bobadilla S, Borowsky RL: **Gene flow and population structure in the Mexican blind cavefish complex (Astyanax mexicanus)**. *BMC evolutionary biology* 2012, **12**:9.

23. Strecker U, Bernatchez L, Wilkens H: **Genetic divergence between cave and surface populations of Astyanax in Mexico (Characidae, Teleostei)**. *Molecular Ecology* 2003, **12**(3):699-710.

24. Jeffery W, Strickler A, Yamamoto Y: **To See or Not to See: Evolution of Eye Degeneration in Mexican Blind Cavefish**. *Integrative Comparative Biology* 2003, **43**:531-541.

25. Jeffery WR: **Evolution and Development in the Cavefish Astyanax**. In: *Current Topics in Developmental Biology*. Edited by Jeffery WR, vol. 86. Burlington: Academic Press; 2009: 191-221.

26. Yamamoto Y, Byerly MS, Jackman WR, Jeffery WR: **Pleiotropic functions of embryonic sonic hedgehog expression link jaw and taste bud amplification with eye loss during cavefish evolution**. *Developmental biology* 2009, **330**(1):200-211.

27. Jeffery W, Strickler A, Guiney S, Heyser D, Tomarev S: **Prox 1 in eye degeneration and sensory organ compensation during development and evolution of the cavefish Astyanax**. *Dev Genes Evol* 2000, **210**(5):223-230.

28. Teyke T: **Morphological differences in neuromasts of the blind cave fish Astyanax hubbsi and the sighted river fish Astyanax mexicanus**. *Brain, behavior and evolution* 1990, **35**(1):23-30.

29. Montgomery JC, Coombs S, Baker CF: **The mechanosensory lateral line system of the hypogean form of Astyanax fasciatus**. *Environmental Biology of Fishes* 2001, **62**(1-3):87-96.

30. Burt de Perera T, Holbrook RI: **Three-dimensional spatial representation in freely swimming fish**. *Cognitive processing* 2012, **13 Suppl 1**:107-111.

31. **The biology of Hypogean fishes**, 1st edn. Dordrecht, The Netherlands: Kluwer Academic Publishers; 2001.

32. Boudriot F, Reutter K: **Ultrastructure of the taste buds in the blind cave fish Astyanax jordani ("Anoptichthys") and the sighted river fish Astyanax mexicanus (Teleostei, Characidae)**. *The Journal of comparative neurology* 2001, **434**(4):428-444.

33. Yamamoto Y, Stock DW, Jeffery WR: **Hedgehog signalling controls eye degeneration in blind cavefish**. *Nature* 2004, **431**(7010):844-847.

34. Popper AN: **Auditory capacities of the mexican blind cave fish (astyanax jordani) and its eyed ancestor (astyanax mexicanus)**. *Animal Behaviour* 1970, **18**(3):552-562.

35. Riedel G, Krug L: **The forebrain of the blind cave fish Astyanax hubbsi (Characidae). II. Projections of the olfactory bulb**. *Brain, behavior and evolution* 1997, **49**(1):39-52.

36. Riedel G: **The forebrain of the blind cave fish Astyanax hubbsi (Characidae). I. General anatomy of the telencephalon**. *Brain, behavior and evolution* 1997, **49**(1):20-38.

37. Peters N, Schacht V, Schmidt W, Wilkens H: **Gehirnproportionen und Ausprägungsgrad der Sinnesorgane von Astyanax mexicanus (Pisces Characinidae): ein Vergleich zwischen dem Flussfisch und seinen Höhlenderivaten «Anoptichthys»**. *Zeitschrift für Zoologische Systematik und Evolutionsforschung* 1993, **31**(2):144-159.

38. Menuet A, Alunni A, Joly JS, Jeffery WR, Retaux S: **Expanded expression of Sonic Hedgehog in Astyanax cavefish: multiple consequences on forebrain development and evolution**. *Development* 2007, **134**(5):845-855.

39. Retaux S, Pottin K, Alunni A: **Shh and forebrain evolution in the blind cavefish Astyanax mexicanus**. *Biology of the cell / under the auspices of the European Cell Biology Organization* 2008, **100**(3):139-147.

40. Demski LS, Knigge KM: **The telencephalon and hypothalamus of the bluegill (Lepomis macrochirus): evoked feeding, aggressive and reproductive behavior with representative frontal sections**. *The Journal of comparative neurology* 1971, **143**(1):1-16.

41. Voneida TJ, Fish SE: **Central Nervous-System Changes Related to the Reduction of Visual Input in a Naturally Blind Fish (Astyanax-Hubbsi)**. *Am Zool* 1984, **24**(3):775-782.

42. Schmatolla E: **Dependence of tectal neuron differentiation on optic innervation in teleost fish**. *Journal of embryology and experimental morphology* 1972, **27**(3):555-576.

43. Voneida TJ, Sligar CM: **A Comparative Neuroanatomic Study of Retinal Projections in Two Fishes: Astyanax hubbsi (the Blind Cave Fish), and Astyanax m exicanus**. *The Journal of comparative neurology* 1976, **165**:89-106.

44. Cahn PH: **Comparative optic development in *Astyanax mexicanus* and in two of its blind cave fish derivatives**. *Bull Am Mus Nat Hist* 1958, **115**(2):69-112.

45. Yamamoto Y, Jeffery WR: **Central role for the lens in cave fish eye degeneration**. *Science* 2000, **289**(5479):631-633.

46. Yamamoto Y, Jeffery WR: **Probing teleost eye development by lens transplantation**. *Methods* 2002, **28**(4):420-426.

47. Soares D, Yamamoto Y, Strickler AG, Jeffery WR: **The lens has a specific influence on optic nerve and tectum development in the blind cavefish Astyanax**. *Developmental neuroscience* 2004, **26**(5-6):308-317.

48. Yoshizawa M, Goricki S, Soares D, Jeffery WR: **Evolution of a behavioral shift mediated by superficial neuromasts helps cavefish find food in darkness**. *Current biology : CB* 2010, **20**(18):1631-1636.

49. Yoshizawa M, Jeffery WR: **Evolutionary tuning of an adaptive behavior requires enhancement of the neuromast sensory system**. *Commun Integr Biol* 2011, **4**(1):89-91.

50. Yoshizawa M, Yamamoto Y, O'Quin KE, Jeffery WR: **Evolution of an adaptive behavior and its sensory receptors promotes eye regression in blind cavefish**. *BMC biology* 2012, **10**(108):108.

51. Purves D, Augustine GJ, Fitzpatrick D, Hall WC, LaMantia A-S, McNamara JO, Williams SM: **Neuroscience**, 3rd edn. Sunderland, Massachussets: Sinauer Associates, Inc.; 2004.

52. Quintana L, Sharpe J: **Optical projection tomography of vertebrate embryo development**. *Cold Spring Harbor protocols* 2011, **2011**(6):586-594.

53. Metscher BD: **MicroCT for comparative morphology: simple staining methods allow high-contrast 3D imaging of diverse non-mineralized animal tissues**. *BMC physiology* 2009, **9**:11.

54. Metscher BD: **MicroCT for developmental biology: a versatile tool for high-contrast 3D imaging at histological resolutions**. *Developmental dynamics : an official publication of the American Association of Anatomists* 2009, **238**(3):632-640.

55. Metscher BD, Muller GB: **MicroCT for molecular imaging: quantitative visualization of complete three-dimensional distributions of gene products in embryonic limbs**. *Developmental dynamics : an official publication of the American Association of Anatomists* 2011, **240**(10):2301-2308.

56. Piotrowski T, Northcutt RG: **The cranial nerves of the Senegal bichir, Polypterus senegalus [osteichthyes: actinopterygii: cladistia]**. *Brain, behavior and evolution* 1996, **47**(2):55-102.

57. Deguchi T, Suwa H, Yoshimoto M, Kondoh H, Yamamoto N: **Central connection of the optic, oculomotor, trochlear and abducens nerves in medaka, Oryzias latipes**. *Zoolog Sci* 2005, **22**(3):321-332.

58. Luiten PG: **The central projections of the trigeminal, facial and anterior lateral line nerves in the carp (Cyprinus carpio L.)**. *The Journal of comparative neurology* 1975, **160**(3):399-417.

59. Raible DW, Kruse GJ: **Organization of the lateral line system in embryonic zebrafish**. *The Journal of comparative neurology* 2000, **421**(2):189-198.

60. Corfield JR, Birkhead TR, Spottiswoode CN, Iwaniuk AN, Boogert NJ, Gutierrez-Ibanez C, Overington SE, Wylie DR, Lefebvre L: **Brain size and morphology of the brood-parasitic and cerophagous honeyguides (aves: piciformes)**. *Brain, behavior and evolution* 2013, **81**(3):170-186.

61. Jolesz F, Sreter FA: **Development, innervation, and activity-pattern induced changes in skeletal muscle**. *Annu Rev Physiol* 1981, **43**:531-552.

62. Patton P, Windsor S, Coombs S: **Active wall following by Mexican blind cavefish (Astyanax mexicanus)**. *Journal of comparative physiology A, Neuroethology, sensory, neural, and behavioral physiology* 2010, **196**(11):853-867.

63. Wilkens H: **Evolution and Genetics of Epigean and Cave Astyanax-Fasciatus (Characidae, Pisces) - Support for the Neutral Mutation Theory**. *Evolutionary biology* 1988, **23**:271-367.

64. Windsor SP, Tan D, Montgomery JC: **Swimming kinematics and hydrodynamic imaging in the blind Mexican cave fish (Astyanax fasciatus)**. *The Journal of experimental biology* 2008, **211**(Pt 18):2950-2959.

65. Laughlin SB, de Ruyter van Steveninck RR, Anderson JC: **The metabolic cost of neural information**. *Nature neuroscience* 1998, **1**(1):36-41.

66. Kotrschal A, Rogell B, Bundsen A, Svensson B, Zajitschek S, Brannstrom I, Immler S, Maklakov AA, Kolm N: **Artificial selection on relative brain size in the guppy reveals costs and benefits of evolving a larger brain**. *Current biology : CB* 2013, **23**(2):168-171.

67. Farnworth M, Schulz-Mirbach T, Riesch R, Bierbach D, Klaus S, Eifert C, Tobler M, Streit B, Indy JR, Arias-Rodriguez L *et al*: **Adaptive divergence of brain morphology in extremophile fish supports mosaic evolution of the teleost brain**. *Biological Journal of the Linnean Society* 2013 **(submitted)**.

68. Romero A, Green SM, Romero A, Lelonek MM, Stropnicky KC: **One Eye But No Vision: Cave Fish With Induced Eyes Do Not Respond to Light**. *J Exp Zool* 2003, **300**:72-79.

69. Friedrich RW, Korsching SI: **Combinatorial and chemotopic odorant coding in the zebrafish olfactory bulb visualized by optical imaging**. *Neuron* 1997, **18**(5):737-752.

70. Sylvester JB, Rich CA, Yi C, Peres JN, Houart C, Streelman JT: **Competing signals drive telencephalon diversity**. *Nature Communications* 2013, **4**:1745.

71. Elipot Y, Hinaux H, Callebert J, Retaux S: **Evolutionary shift from fighting to foraging in blind cavefish through changes in the serotonin network**. *Current biology : CB* 2013, **23**(1):1-10.

72. Broglio C, Rodriguez F, Salas C: **Spatial cognition and its neural basis in teleost fishes**. *Fish and Fisheries* 2003, **4**(3):247-255.

73. Charvet CJ, Striedter GF: **Developmental basis for telencephalon expansion in waterfowl: enlargement prior to neurogenesis**. *Proceedings Biological sciences / The Royal Society* 2009, **276**(1672):3421-3427.

74. Vaccarino FM, Schwartz ML, Raballo R, Nilsen J, Rhee J, Zhou M, Doetschman T, Coffin JD, Wyland JJ, Hung Y-TE: **Changes in cerebral cortex size are governed by fibroblast growth factor during embryogenesis**. *Nature neuroscience* 1999, **2**(3):246-255.

75. Israsena N, Hu M, Fu W, Kan L, Kessler JA: **The presence of FGF2 signaling determines whether beta-catenin exerts effects on proliferation or neuronal differentiation of neural stem cells**. *Developmental biology* 2004, **268**(1):220-231.

76. Kang W, Wong LC, Shi SH, Hebert JM: **The transition from radial glial to intermediate progenitor cell is inhibited by FGF signaling during corticogenesis**. *The Journal of neuroscience : the official journal of the Society for Neuroscience* 2009, **29**(46):14571-14580.

77. Glover JC, Petursdottir G, Jansen JKS: **Fluorescent dextran-amines used as axonal tracers in the nervous system of the chicken embryo**. *Journal of Neuroscience Methods* 1986, **18**:243-254.

Supplements

Material and Methods

Acetylated α-tubulin staining for Micro-CT imaging

For CN measurements and reconstructions at the 5 day stage, the initial idea was to use Micro-CT to image embryos stained for Acetylated α-tubulin (Aαt) by following the method developed by Metscher et al. [55]. 5 day old surface fish and pachón previously fixed in PFA 4% and stored in methanol overnight at -20°C were treated with 3% hydrogen peroxide in methanol for 30 min to eliminate endogenous peroxidase activity. They were then rehydrated through a methanol series (75%, 50%, 25%, 5 min each) to MABT (100 mM maleic acid, 150 mM NaCl, 0.1% Triton X-100, pH 7.4) and then washed 10 min in MABT + 0.1% saponin. Afterwards, the samples were digested in proteinase K, 20µg/ml in MABT + 0.1% saponin for 20 min at room temperature and post-fixed in PFA 4% for 20 min at room temperature as well. After three 5 min washes in MABT + 0.1% saponin, they were then blocked for 1 hour at room temperature with blocking solution (MABT with 0.1% saponin, 10% goat serum, 0.5% Roche Blocking Reagent, and 1% dimethylsulfoxide). This step was followed by the overnight 4°C incubation of primary mouse anti-Aαt antibody (Invitrogen), diluted 1:2000 in the same blocking solution. Samples were then changed to blocking solution for 1 hour and then to secondary antibody (goat anti-mouse IgG HRP conjugate, Invitrogen F21453), diluted 1:1000 in blocking solution, and left overnight at 4°C. In the next day, samples were rinsed 3 times in MABT + 0.1% saponin, and then 6 times 30 min in the same solution, and left washing overnight in the rocker at room temperature. Samples were, again, post-fixed in 4% PFA for 20 min at room temperature, washed 3 times in double distilled water (ddH_2O) for 10 min each, then changed to 0.1% Triton X-100 in ddH_2O.

After transferring the samples to new rinsed tubes, the enzyme metallography kit (EnzMet™, Nanoprobes) with the purpose of creating x-ray contrast in the sites were the secondary antibody was located. Through chemical reduction with the peroxidase reactions, dissolved silver ions (Ag^+) are reduced to insoluble metallic silver (Ag^0), which precipitate in the vicinities of the enzyme conjugate. This allows a peroxidase-conjugated secondary antibody to be visualized by applying a metal ion solution (silver acetate), followed by a reducing agent (hydroquinone), and followed by an electron acceptor (hydrogen peroxide). All three solutions are part of the EnzMet™ kit and were sequentially added (300 µL each) to the samples which were in 300 µL of ddH_2O + 0.1% Triton X-100. After adding the last solution of the kit, the staining was monitored under a stereomicroscope and reactions were stopped with 1% sodium thiosulfate in ddH_2O + 0.1% Triton X-100. The staining period was in between 30 min and 45 min.

For imaging, samples were serially dehydrated to 100% ethanol, mounted in polypropylene micropipette tips, sealed and capped with Blu Tack (Bostik) [53]. The scanning settings used for these samples were the same as the ones used for the PTA stained 5 dpf fish. However, the scanner was never able to detect the staining and it only detected some silver agglomerates in the surface of the scanned samples, not in the cranial nerves – even if the staining was evident in the dissecting microscope.

Acetylated α-tubulin DAB staining

To control for some of the problems that arose with the Enzyme Metallography staining, a DAB staining was performed. It was chosen in order to make use of the same antibodies and it was done using the same protocol as above and by doing it in alternative way. Prior to the rehydration to PBT (PBS + 0.1% Triton X-100), samples were treated with 30% hydrogen peroxide in methanol for 30 min. Samples were then washed in PBT (5 min, 2 times) and then blocked for 1 hour in Super Block (2% Roche Blocking Reagent, 2% Bovine Serum Albumin, 10% Goat Serum

in MABT) and Avidin Block (Vector) at room temperature. After more PBT washes, samples were incubated overnight at 4°C with primary antibody (mouse anti-Aαt, Invitrogen), 1:2000 with Biotin Block (Vector) in Super Block. Next day, following washes in PBT (5, 10, 20 and 30 min, in this order), samples were again incubated in Super Block for 1 hour before overnight 4°C incubation with the secondary antibody (goat anti-mouse IgG HRP conjugate, Invitrogen F21453), diluted 1:500. Samples were then washed in PBT, transferred to PBS 1x and incubated for 1 hour with ABC Solution (Vector). After washing with PBST (PBS + 0.1% Tween 20), the DAB Kit (Vector) was used to stain the samples. The staining was monitored under the stereomicroscope and when the fish were stained enough (after approximately 30 min), the samples were fixed in PFA 4% at room temperature for 30 min. Pictures of the stained samples were taken using a Nikon Stereomicroscope SMZ1500 and pictures were taken using a Nikon DS-2M camera head and a Nikon Digital Sight DS-U1 camera controller.

OPT preparation and imaging

We briefly tried to use OPT procedure to understand if it could actually fit the purpose of this project. Therefore, by following standard methodology [52], 5 dpf surface and cavefish larvae were imaged following and rhodamine dextran amine (RDA, Invitrogen) and fluorescent dextran amine (FDA, Invitrogen) injections to the brain [77]. All fish were previously fixed in PFA 4% and dehydrated to methanol prior to FDA and RDA injections. After 24h in PBS 1x at room temperature, samples were then prepared accordingly: the larvae were embedded in a block 1% low melting point agarose (Sigma) in PBS which was then trimmed. After dehydration in methanol, sample were cleared in BABB (1:2 Benzyl Alcohol and Benzyl Benzoate) before imaging. Imaging was performed in the Bioptonics 300M Scanner, and alignment and reconstruction software were also provided the same company.

Paraffin sectioning, immunohistochemistry and reconstruction

As an alternative for the micro-CT imaging of 5 dpf stage CN, paraffin sections and subsequent Aαt immunohistochemistry was performed. Both surface and pachón fish at that stage, previously fixed and stored overnight in methanol at -20°C, were transferred to 100% ethanol for 1 hour and then to butanol for another hour. Afterwards, samples were transferred to paraffin at 60°C and the paraffin was changed 4 times every 30 min to remove all butanol. Samples were then embedded into paraffin blocks and left overnight at room temperature. Embedded samples were then taken to the microtome and sectioned at 10µm. Sections were then mounted in Superfrost Plus coated slides (Thermo Scientific) and rehydrated at 40°C in a hot plate for exactly 3 min (all slides had to stay exactly the same so that the expansion they undergo during rehydration can be roughly the same in all sections). Sections were then left to dry at room temperature (or slightly higher) overnight. All sections were washed in Xylene (3 times, 10 min) and then serially rehydrated from ethanol to PBS 1x (100%, 95%, 90%, 80%, 70%, 50% and PBS 1x). After this step, all the slides were taken to a pressure cooked in unmasking solution (Vector) at 1:100 in ddH_2O for 3 min and then blocked for 1 hour in TNB (10% TRIS 1M, 3% NaCl 5M, 0.5% Blocking Reagent (Perkin Elmer) in ddH_2O). Sections were then incubated overnight at room temperature in the primary antibody (mouse anti-Aαt, Invitrogen), diluted at 1:50 in TNB – this dilution value was chosen for the quality of the fluorescence after trying several others. Next day they were washed in PBS (5 times, 30 min) and then incubated for 4 hours at room temperature in the secondary antibody (Alexa Fluor® 488 goat anti-mouse IgG, Invitrogen) diluted 1:200 in TNB. All sections were then washed in PBS and mounted in PBS/Glicerol medium (1:1) and imaged in a Nikon Stereomicroscope SMZ1500 with a Nikon DS-2M camera head and a Nikon Digital Sight DS-U1 camera controller. All images were then loaded onto Amira 5.3.3 (Visage Imaging), aligned and stacked to performed 3D reconstruction of the CN. However, due to the fact the sections were detaching from the slides, reconstruction was not possible. To solve this issue, the pressure cooking step was replaced by an overnight wash in PBS+1% Triton X-100, but the sections were still detaching from the slide. To control for a

possible problems in the glass slides, another batch was used and uncoated slides were also manually coated with AAS (Sigma) prior to mounting. Unfortunately the problem still remained.

Lens deletion in surface fish

Lens deletion was performed with the goal of detecting brain changes related with the lack of visual input. These were performed following the method developed by Yamamoto et al. [46]. Surface fish embryos between 36-40 hpf were transferred into calcium free ringer for 5 and 15 min, sequentially, and then washed for 20 min in 0.2% EDTA in calcium free ringer to remove all calcium ions necessary for calcium-dependent cell adhesion. After another wash, they were then transferred to 1.2% agarose in the same ringer, and placed on their lateral side in a petri dish. Using tungsten needles, the lens of one eye was removed from the immobilized fish carefully enough to not damage vessels or the brain. The other eye was left untouched as a control. Lens transplantations between surface fish embryos were also performed as a control for the manipulation. After the procedure, normal ringer was added to allow the wounds to close, and after recovery, fish were released from the agar and transferred to E2 medium to carry on their development. Pictures of operated and control eyes were taken in the day after the procedure to screen for unsuccessful manipulations. Lens deletions in both eye were also performed in some surface fish. For this case, the entire method described before was applied to the eye of one side of the fish and, after recovery, the other eye would be operated on. Fish were then sacrificed at 5 dpf or would be raised normally to fully mature adults. All manipulations and photographs were made with a Nikon Stereomicroscope SMZ1500 with a Nikon DS-2M camera head and a Nikon Digital Sight DS-U1 camera controller.

Supplemental Figures

Cranial nerve 5 dpf

Cranial nerves at 5 dpf were analysed. However, the overall measures were not normalized with the fish's volume. For this reason, no differences were probably found at this stage (Mann-Whitney U, $p>0.05$), even though the graphs already suggest some differences, particularly the vagus (S.Fig.2) and trigeminal (S.Fig.1)

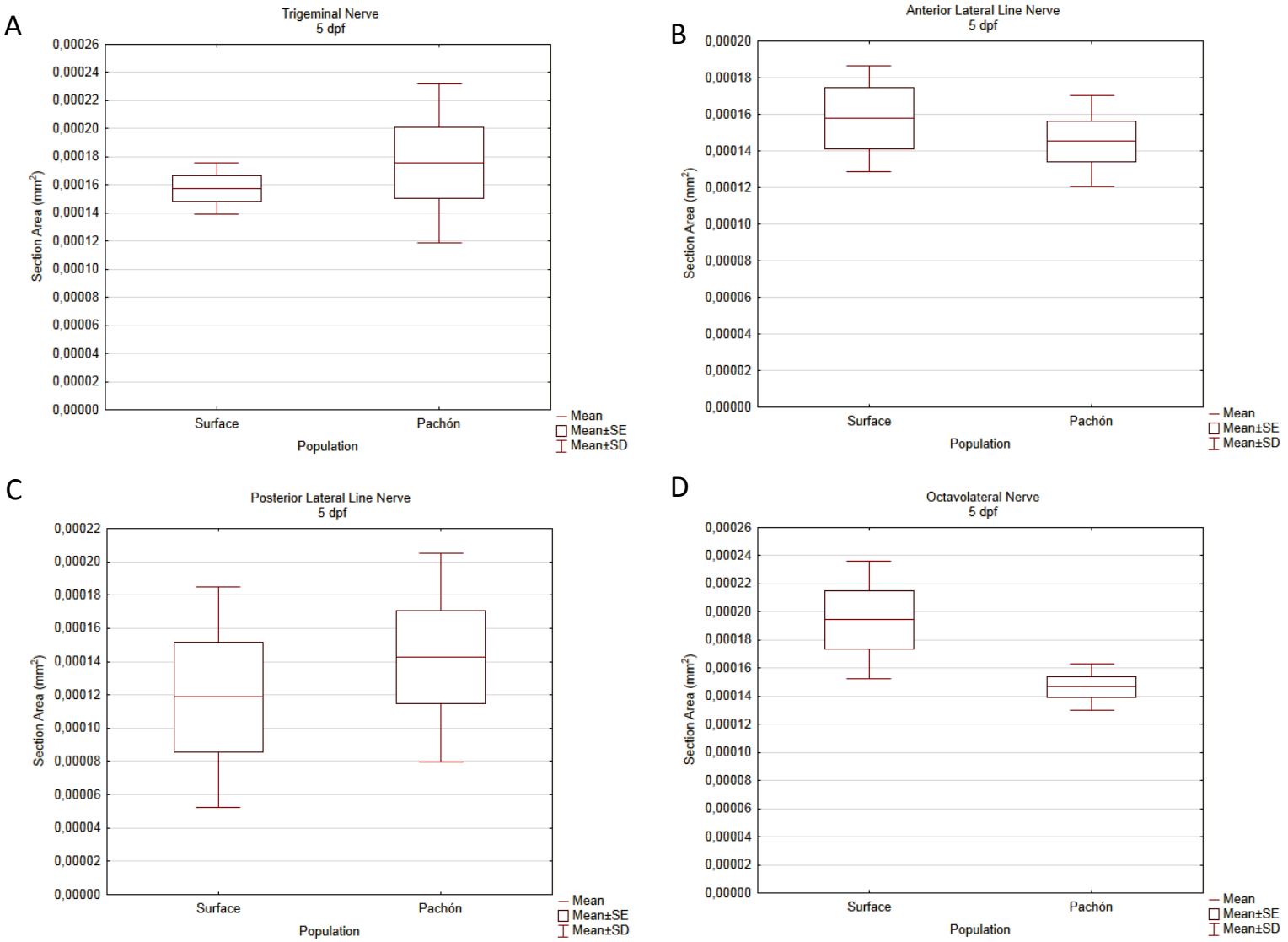

S. Figure 1 – Boxplot graphs showing the differences in section area of CNV (A), ALLN (B), PLLN (C) and CNVIII (D) between the two morphotypes at 5 dpf. Boxplots were constructed using mean, standard error and standard deviation.

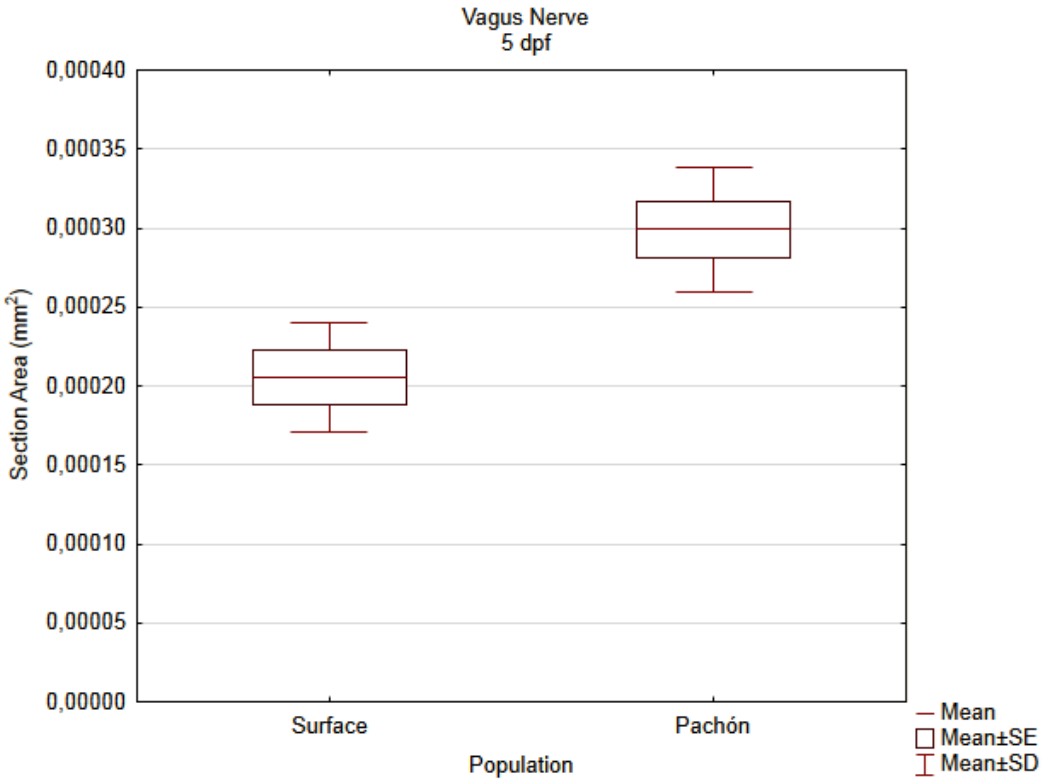

S. Figure 2 – Boxplot graph showing the differences in section area of CNX between the two morphotypes at 5 dpf. Boxplots were constructed using mean, standard error and standard deviation.

Ratios of different regions across stages

TeO comparison between different ages show significant differences (Mann-Whitney U, p=0.008 for both Surface and Pachón). However, from 5 dpf to 1 ypf, the tectal ratio is reduced in the Pachón (S.Fig.4 C) and increased in the surface fish (S.Fig.4 A). The telencephalic ratio shows significant increases (S.Fig.3) in both Pachón and surface populations (Mann-Whitney U, p=0.008 and p=0.014, respectively). The hypothalamic ratio in the surface fish analysed suffers a decrease (ANOVA, p=0.0011), while no significant differences appear between both stages in the Pachón cavefish (S.Fig.4 B and D, respectively).

Ratios at 5 days without the Tectum

The 5 dpf telencephalic and hypothalamic volumes were individually normalized by the whole brain volume without the TeO's volume. As a result, the hypothalamus shows significant differences between both morphotypes (ANOVA, p=0.012), being bigger in the surface fish. (S.Fig.5).

Adult Ratios with identical TeO in both Morphotypes

In order to determine whether our previous calculations of the different ratios excluding the TeO did in fact demonstrate an apparent scale-down cerebellum, hypothalamus and telencephalon, we proportionally increased the tectal volume in the Pachón morphotype by roughly adding another tectum to the total brain volume (as the decrease in tectal ratio in the adult is of about 55%). As a result, the recalculated ratios indicate the same as before, all structures but the OB seem appear to have suffered no relative expansions, just an overall decrease in volume (S.Fig.6).

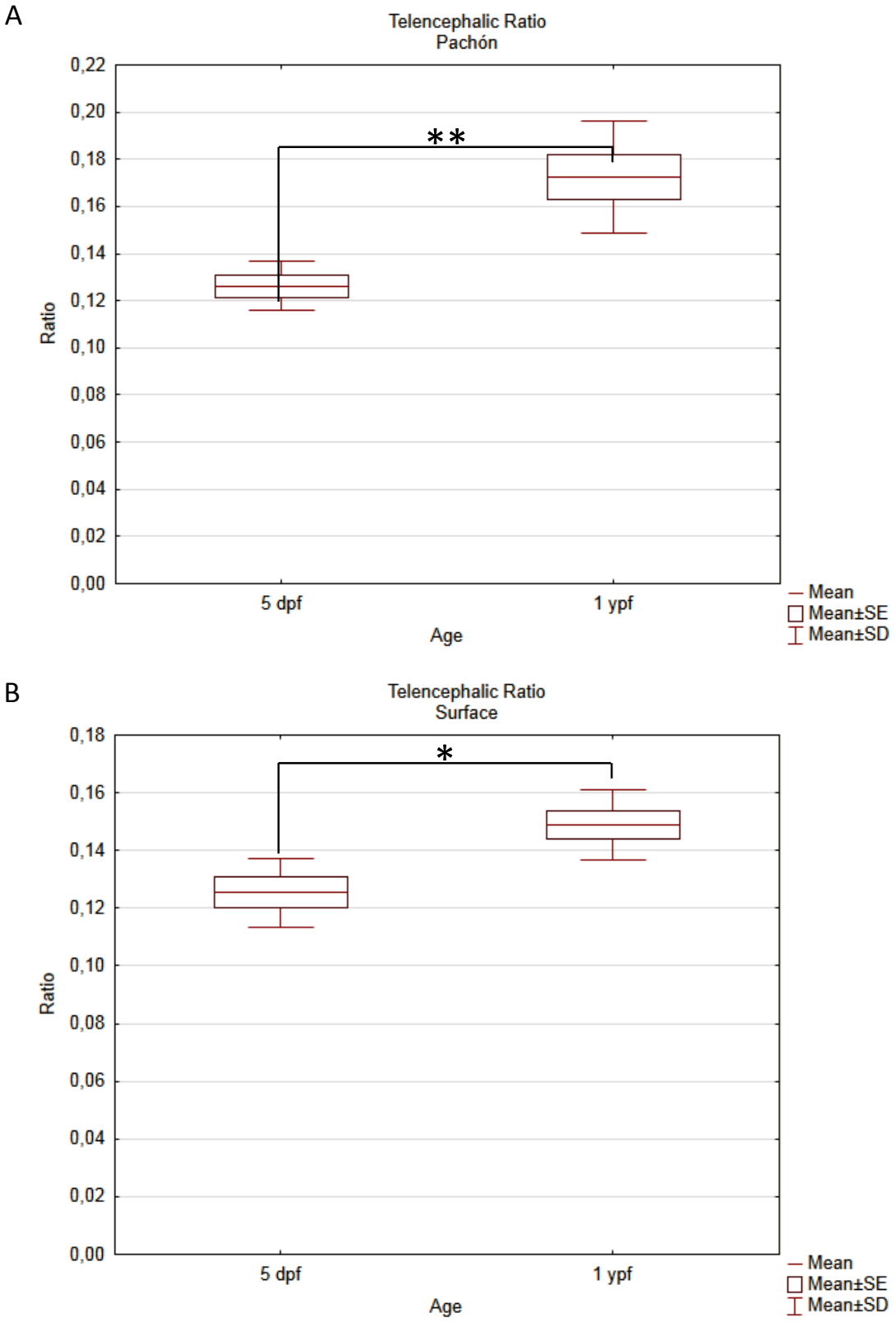

S. Figure 3 – Boxplot graphs showing the differences in telencephalic ratios between the two analysed stages in both Pachón (A) and surface (B) populations. Boxplots were constructed using mean, standard error and standard deviation. Significance is shown where relevant (* for $p<0.05$, ** for $p<0.01$;).

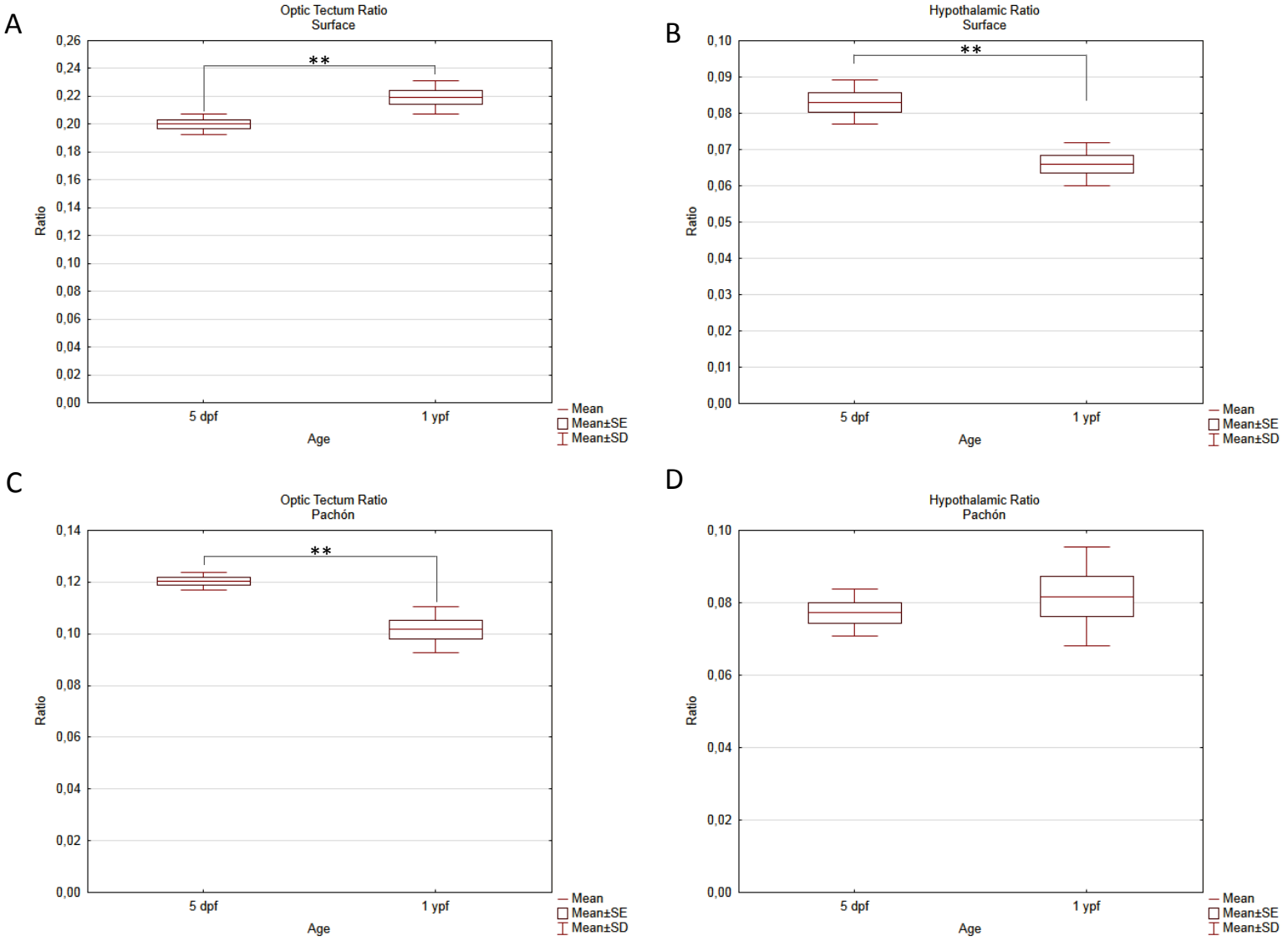

S. Figure 4 – Boxplot graphs showing the differences in tectal (A and C) and hypothalamic (B and D) ratios between the two analysed stages in both Pachón (C and D) and surface (A and B) populations. Boxplots were constructed using mean, standard error and standard deviation. Significance is shown where relevant (* for $p<0.05$, ** for $p<0.01$;).

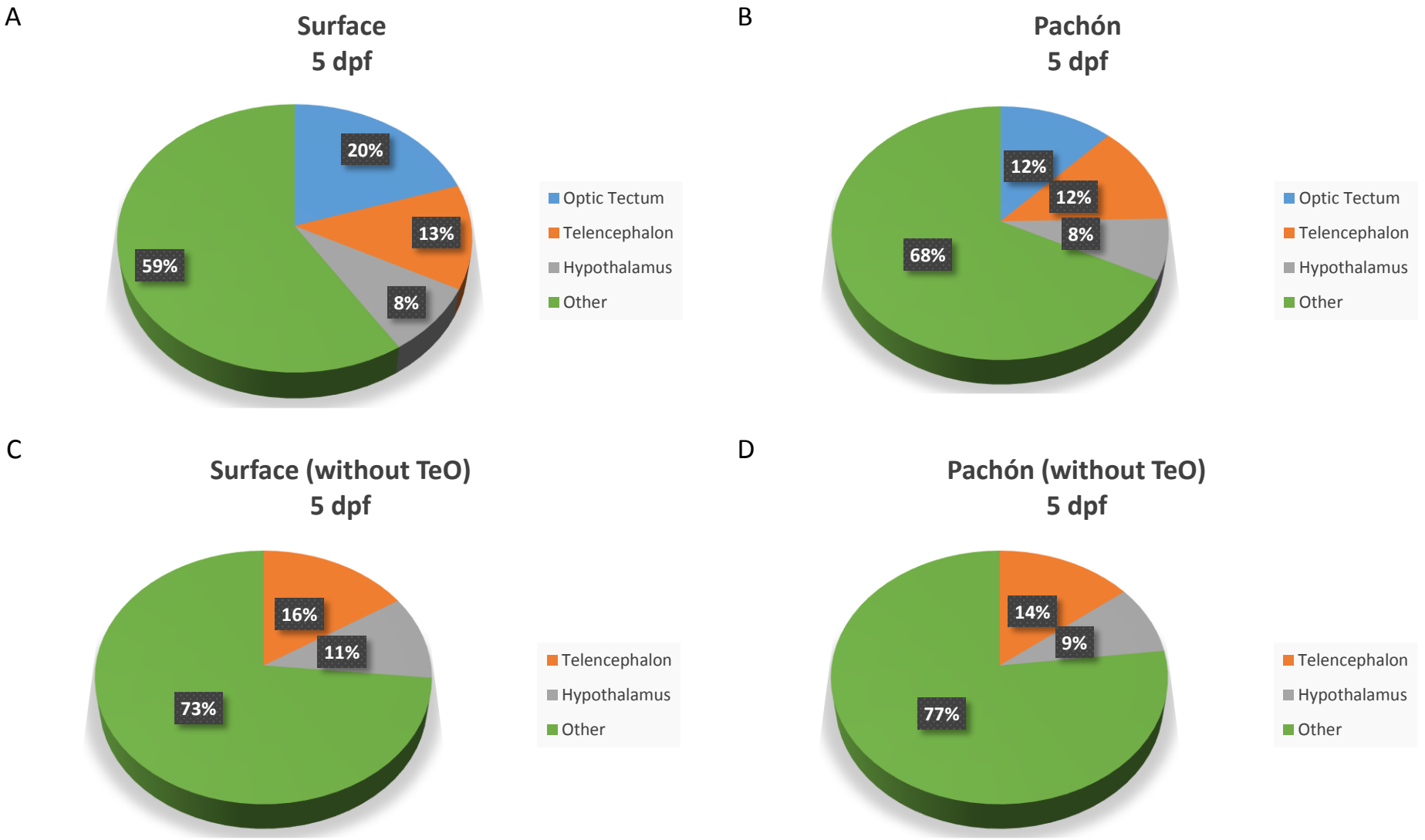

S. Figure 5 – Pie charts showing the different ratios of each analysed brain region in the 5 dpf stage. A and B represent the mean ratios measured for each region, previously compared between both morphotypes. C and D are the mean ratios for each region calculated by excluding the tectal volume from the overall brain volume. Only the recalculated hypothalamic ratio (C and D) shows significant differences (ANOVA, p=0.012).

A

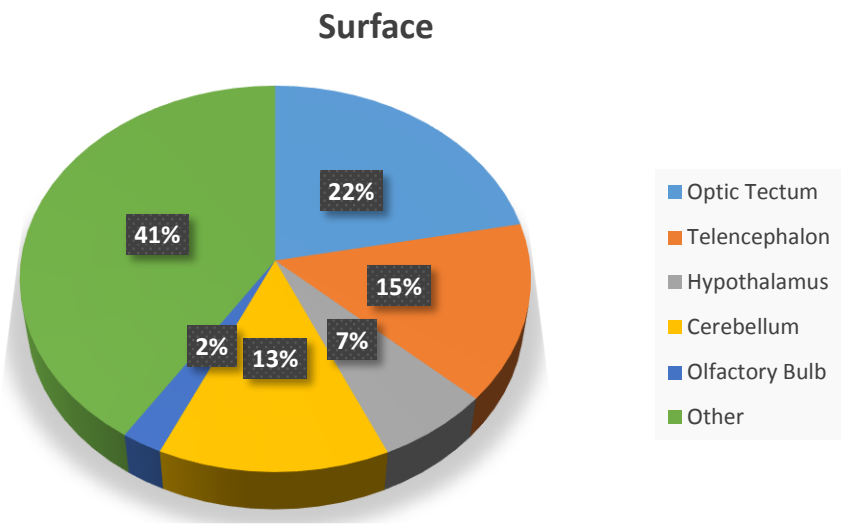

B

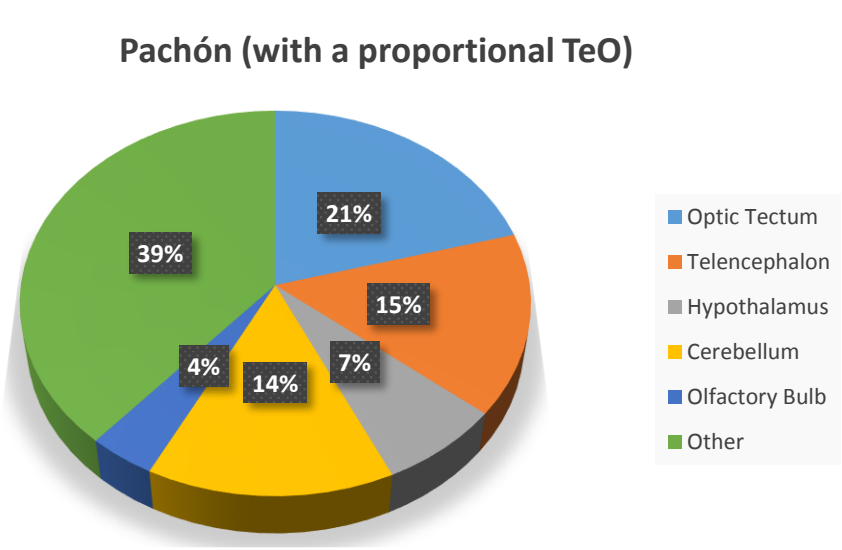

S. Figure 6 – Pie charts showing the different ratios of each analysed brain region in adult fish. A corresponds to the unchanged surface fish ratios and B corresponds mean ratios for each region calculated by adding the missing tectal volume to the overall brain volume. No differences are found between both morphotypes when this ratio is measured (ANOVA, $p>0.05$) except for the OB which remains specifically bigger in the Pachón (ANOVA, $p<0.001$).